4

EA Against Modern Radar Systems

In this chapter, we examine EA against several of the most important advanced techniques employed in modern radar. These include *pulse compression* (PC), *pulse Doppler* (PD), monopulse, *ultralow sidelobe antennas* (ULSAs), and *coherent sidelobe cancellation* (CSLC). All these techniques make modern radars difficult to jam and require special EA techniques for effective jamming.

The use of PC and pulsed Doppler in radar systems represents the use of both intra- and interpulse coherence in the radar waveform. This produces not only improved radar performance but also a resistance to jamming waveforms that are mismatched to the radar transmitted waveform. This trend is driven by the rapid advancements in digital signal processing and the availability of stable microwave amplifiers. Both techniques provide a potentially large processing gain against noise-type signals. With PC, the processing gain is equal to the time-bandwidth product of the radar waveform, which might range from 30 (i.e., 15-dB gain) in older radars to over 1000 (i.e., 30-dB gain) in more modern radars. Pulse Doppler radars exhibit a similar processing gain equal to the product of the CPI and the radar's PRF. For example, if the radar's PRF were 50 kHz and the CPI were 20 ms, then the processing gain against noise would be 1000 or 30 dB. In principle, both techniques are compatible [1] and the processing gains in decibels are additive.

Monopulse is used primarily in target tracking radars and missile seekers. Its mechanization provides an inherent resistance to amplitude-modulated jamming waveforms that tends to limit jamming from point sources. Fundamental EA techniques against monopulse generally employ dual spatially displaced coherent sources [2] such as cross-eye, terrain bounce, and blinking [3]. Cross-polarization jamming can also be used to exploit weaknesses in certain forms of monopulse tracking systems susceptible to this technique. These

include reflector-type antennas, small flat plate arrays susceptible to edge effects, and any antenna in an aircraft or missile radome.

ULSAs and CSLCs are forms of spatial filtering that eliminate jamming signals from the radar's sidelobe response. ULSA antennas are a proven operational technique that provide average sidelobes the order of −20 dBi or lower. ULSAs use a combination of careful aperture illumination design and control of mechanical tolerances to create a low sidelobe design. CSLCs are a form of adaptive antenna array processor that forms a null on jammers in the radar's sidelobes. Generally, one null can be formed due to the interferometric action between the main antenna and any auxiliary antennas employed. Thus, each auxiliary antenna deployed provides the potential for canceling one sidelobe jammer. CSLCs generally provide processing gains of the order of 20 dB to 30 dB, but their theoretical performance is potentially much higher [3]. A CSLC can be employed with an ULSA to provide a high degree of resistance to sidelobe jamming but tend to be generally applied with conventional sidelobe antennas.

4.1 PC

The basic concept of a PC waveform is to transmit a long pulse of duration τ_d with bandwidth B and process the target return in a matched filter that compresses the long pulse to a short pulse of duration $\tau_s = 1/B$. Since the matched filter is theoretically lossless, the energy at the input to the matched filter ($S \cdot T$) must equal that at its output (P_{pc}/B). Thus, at the output of the matched filter, the pulsed compression power is given by

$$P_{pc} = (B \cdot T)S \tag{4.1}$$

where

S = received peak power

B = transmitted bandwidth

T = transmitted pulse width

The time-bandwidth product

$$\beta = BT \tag{4.2}$$

is a measure of the increase in peak power due to the PC. Note that for detection calculation purposes, either the uncompressed pulse factors (S, T) or the compressed pulse factors (P_{pc}, τ_s) give the same result since they contain

the same energy. In fact, any system using a matched filter processor provides an output signal-to-noise ratio equal to $2E_R/\eta_o$, where E_R is the pulse energy ($S \cdot T$) and η_o is the spectral density of the white receiver noise.

When noise jamming is employed, the PC network generally provides an advantage that is equal to the PC ratio $T \cdot B$, where the comparison is against a conventional radar with equal transmitter energy and matched jammer bandwidth. This can be rationalized by considering the matched filter signal-to-noise ratio $2E_R/\eta_o$, which is the same for both PC and conventional radar of equal transmitted energy. However, the jammer must support a bandwidth of B against the PC radar, resulting in a jammer power of $B \cdot \eta_o$ as compared to a bandwidth of $1/\tau$ for the conventional radar, resulting in a jammer power of η_o/τ. The ratio of the jammer powers for the PC radar as compared to the conventional radar is, therefore, the PC ratio $T \cdot B$, assuming that a narrow spot bandwidth $1/\tau$ would be usable for the conventional radar.

Common forms of PC waveforms are the linear FM and phase-coded types. With linear FM, the bandwidth of the waveform is closely approximated by the difference between the minimum and maximum frequencies of the chirp waveform. With phase-coded waveforms, which are similar to spread-spectrum communication signals, the PC bandwidth can be approximated by the chip rate.

A matched filter that processes signal $v(t)$ has a conjugate impulse response given by $v^*(-t)$. The output of the matched filter is then given by the convolution integral as

$$g(t) = \int_{-\infty}^{\infty} v(\tau)v^*(t - \tau)\, d\tau \tag{4.3}$$

which is also the *autocorrelation function* (ACF) of the signal. The Fourier transform of the matched filter output is given by the power spectral density $V(\omega) \cdot V^*(\omega) = |V(\omega)|^2$, where $V(\omega)$ is the Fourier transform of the signal. The output signal can alternatively be found as

$$g(t) = \frac{1}{2\pi}\int_{-\infty}^{\infty} |V(\omega)|^2 e^{j\omega t}\, d\omega \tag{4.4}$$

4.1.1 Linear FM Pulse Compression

A linear FM signal can be expressed in complex form as

$$\tilde{v}_t = \exp\left[-j\left(\omega_0 t + \frac{\alpha t^2}{2}\right)\right] \qquad -\frac{T}{2} < t < \frac{T}{2} \tag{4.5}$$

where

$$\alpha = 2\pi\frac{B}{T} \tag{4.6}$$

is the chirp slope. The instantaneous frequency of the signal is given by

$$f = \frac{1}{2\pi}\frac{d\phi}{dt} = f_0 + \frac{B}{T}t \tag{4.7}$$

The matched filter impulse response of the PC matched filter is given by

$$h(t) = v^*(-t) = \exp\left[-j\left(\omega_0 t - \frac{\alpha t^2}{2}\right)\right] \tag{4.8}$$

which indicates that the impulse response of the matched filter is the signal waveform with negative slope.

▶ *Example 4.1*

Using the complex representation for a linear FM signal given by

$$\tilde{s} = \cos\frac{\alpha t^2}{2} - j\sin\frac{\alpha t^2}{2} \tag{4.9}$$

1. Plot the PC power spectral density for a pulsewidth of 100 μs and a chirp band of 1 MHz (β = 100). What is the chirp bandwidth for this case?
2. Plot the matched filter output response on a logarithmic scale (dB). How far is the first-order sidelobe down from the main-lobe response? Why does this response resemble a $\sin(x)/x$ function?

```
% PULSE COMPRESSION SPECTRUM USING FFT
% ------------------------------------
% pcspec.m

clear;clf;clc;

% Input Chirp Bandwidth and Pulsewidth
```

```
bw=1e6;    % Bandwidth - Hz
T= 1e-4;   % Pulsewidth - sec

%Input FFT Points

lfft=1024;

% Set Time Base

t=-T/2:T/(lfft-1):T/2;

% Sample Complex Chirp

s= exp(-j*pi*bw*t.*t/T);

% Plot Chirp Waveform

subplot(221);
plot(t,real(s));grid;
title(['Chirp Waveform']);

% Find Fourier Spectrum of Chirp

ZY= fft(s,lfft);
Y=fftshift(ZY);

% Find Power Spectral Density

Psd=Y.*conj(Y)/lfft;
A=ceil(max(Psd));
l=length(Y);
f=(1/T)*(-(l-1)/2:(l-1)/2);

% Plot Power Spectral Density

subplot(222);
plot(f,Psd/A);grid
axis([-bw bw 0 1]);
title(['Pulse Compression Spectrum']);
xlabel('Frequency - Hz');
ylabel('Amplitude');

% Find Matched Filter Time Waveform

zh=ifft(Psd,lfft);
h=fftshift(zh);

%Plot Time Waveform

subplot(223);
plot(t,abs(h));grid;
```

```
axis([-T/16 T/16 0 1 ]);
title(['PC Matched Filter Output']);
xlabel('Time - Sec');ylabel('Amplitude');

%Plot Log of Time Waveform

zz=20*log10(abs(h));
subplot(224);
plot(t,zz);grid;
axis([ -T/16 T/16 -60 0]);
title(['PC Matched Filter Output']);
xlabel('Time - Sec');ylabel('Amplitude - DB');
```

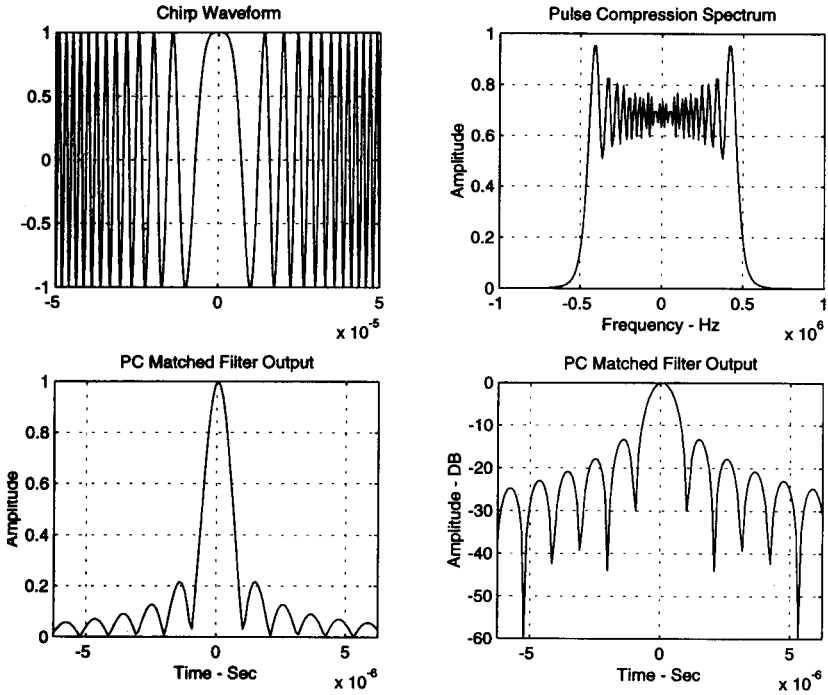

Example 4.1 shows that the output of the matched filter for a linear FM signal has relatively high time sidelobes. These time sidelobes are undesirable since small targets in the vicinity of large targets may be shadowed and go undetected. The solution to this problem is to weight the amplitude of the linear-FM signal with a window function [4]. However, as the sidelobes are reduced by windowing, the width of the main lobe of the PC signal is increased. Also, it is practically difficult to apply the window functions in the time

domain, so they are generally applied in the frequency domain by modifying the frequency response of the matched filter.

▶ *Example 4.2*

Extend Example 4.1 to apply Hamming, Hanning and Blackman window functions to reduce the time sidelobes at the output of a linear-FM matched filter. The weightings are given by

$$\begin{aligned}
&\text{Hamming:} \quad w(k) = 0.54 + 0.46\cos\left(2\pi\frac{k}{N}\right)\\
&\text{Hanning:} \quad w(k) = 0.5\left(1 + \cos\left(2\pi\frac{k}{N}\right)\right)\\
&\text{Blackman:} \quad w(k) = 0.42 + 0.5\cos\left(2\pi\frac{k}{N}\right) + 0.08\cos\left(2\pi\frac{2k}{N}\right)\\
&\text{where} \qquad k = -\frac{N}{2}, \ldots, +\frac{N}{2}
\end{aligned} \tag{4.10}$$

1. Plot the linear-FM matched filter response for Hamming, Hanning, and Blackman windows on a logarithmic scale. What are the relative time sidelobes and main-lobe widths for the various weighting?
2. Apply a Hamming window to the linear-FM chirp filter in the frequency domain. Plot the output power spectral density and matched filter time response. What time sidelobes and lobe spreading result from frequency windowing? Why are they different than time windowing?

```
% Pulse Compression Spectrum with Windows
% ---------------------------------------
% pcwina.m

clear;clf;clc;

% Input Chirp Bandwidth and Pulsewidth

bw=1e6;    % Bandwidth - Hz
T=1e-4;    % Pulse Width - sec

%Input FFT Points
```

```
lfft=1024;

% Set Time Base

t=-T/2:T/(lfft-1):T/2;

% Sample Complex Chirp

s= exp(-j*pi*bw*t.*t/T);

% Window Sample Chirp

w1=1;                                          % Uniform Weighting
w2=.54+.46*cos(2*pi*t/T);                      % Hamming Weighting
w3=.5*(1+cos(2*pi*t/T));                       % Hanning weighting
w4=.42+.5*cos(2*pi*t/T)+.08*cos(4*pi*t/T);    % Blackman Weighting

sw1=s.*w1;sw2=s.*w2;sw3=s.*w3;sw4=s.*w4;

% Find Fourier Spectrum of Chirp

ZY1=fft(sw1,lfft);ZY2=fft(sw2,lfft);
ZY3=fft(sw3,lfft);ZY4=fft(sw4,lfft);
Y1=fftshift(ZY1);Y2=fftshift(ZY2);
Y3=fftshift(ZY3);Y4=fftshift(ZY4);

% Find Power Spectral Density

Psd1=Y1.*conj(Y1)/lfft;
Psd2=Y2.*conj(Y2)/lfft;
Psd3=Y3.*conj(Y3)/lfft;
Psd4=Y4.*conj(Y4)/lfft;

% Find Matched Filter Time Waveform

zh1=ifft(Psd1,lfft);zh2=ifft(Psd2,lfft);
zh3=ifft(Psd3,lfft);zh4=ifft(Psd4,lfft);

h1=fftshift(zh1);h2=fftshift(zh2);
h3=fftshift(zh3);h4=fftshift(zh4);

% Plot Log of Time Waveform

zz1=20*log10(abs(h1));
zz2=20*log10(abs(h2));
zz3=20*log10(abs(h3));
zz4=20*log10(abs(h4));

C1=max(zz1);C2=max(zz2);
C3=max(zz3);C4=max(zz4);

subplot(221);
plot(t,zz1-C1);grid;
axis([ -T/16 T/16 -40 0 ]);
```

```
title(['PC Matched Filter - Uniform']);
xlabel('Time - Sec');ylabel('Amplitude - DB');

subplot(222);
plot(t,zz2-C2);grid;
axis([ -T/16 T/16 -80 0 ]);
title(['PC Matched Filter - Hamming']);
xlabel('Time - sec');ylabel('Amplitude - dB');

subplot(223);
plot(t,zz3-C3);grid;
axis([ -T/16 T/16 -80 0 ]);
title(['PC Matched Filter - Hanning']);
xlabel('Time - sec');ylabel('Amplitude - dB');

subplot(224);
plot(t,zz4-C4);grid;
axis([ -T/16 T/16 -120 0 ]);
title(['PC Matched Filter - Blackman']);
xlabel('Time - sec');ylabel('Amplitude - dB');
```

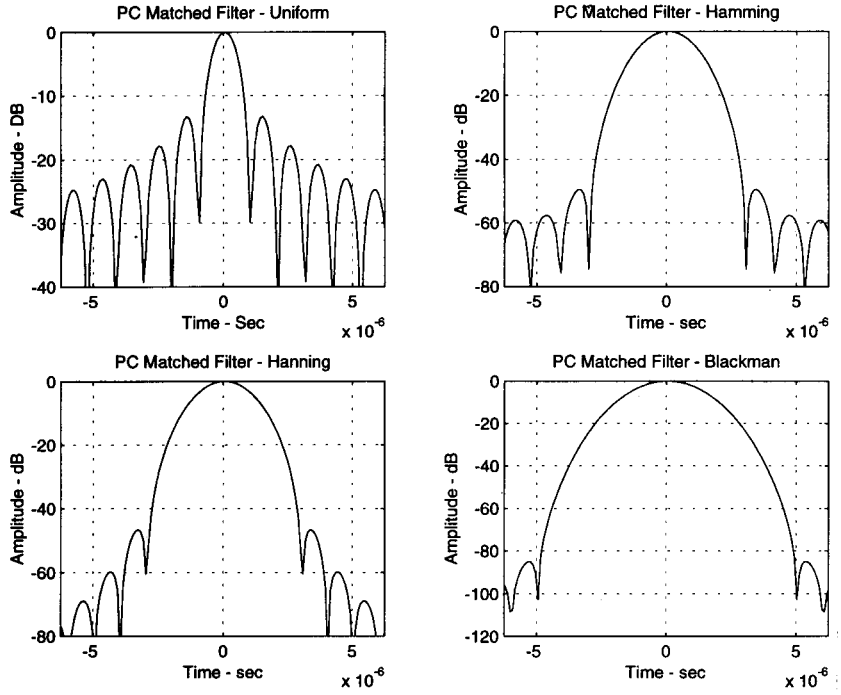

From Example 4.2, it is possible to deduce the resolution properties of the linear-FM waveform with different window functions at the output of the

matched filter in the time domain. Applying the window function reduces the time sidelobes but increases the main lobe response width, thus making it more difficult to resolve two closely spaced targets. When a Doppler shift is present on the received signal, the filter is no longer matched and the output signal is distorted from its original form. The response of the matched filter to a range of frequencies can be determined by plotting the ambiguity function diagram for a particular waveform. In a three-dimensional plane, this diagram displays the response to time delay (range) in one dimension, Doppler shift (frequency shift) in an orthogonal direction, and the magnitude of the receiver response in the third orthogonal direction. The output of the matched filter can be expressed as

$$X(t_d, f_d) = \int_{-\infty}^{\infty} v^*(t) \cdot v(t - t_d) \cdot e^{j2\pi f_d t}\, dt \tag{4.11}$$

where t_d is the range delay and f_d is the Doppler frequency. Alternately, by applying Parseval's theorem, it can be expressed as

$$X(t_d, f_d) = \int_{-\infty}^{\infty} V^*(f) \cdot V(f - f_d) \cdot e^{j2\pi f t_d}\, df \tag{4.12}$$

The ambiguity function is then the squared magnitude $|X(t_d, f_d)|^2$.

► *Example 4.3*

Using MATLAB, plot the ambiguity function for a linear V-FM PC signal. The importance of this waveform is that it is the most basic FM pulse-compression function that yields uncorrelated measurements of range and velocity. It is formed by breaking the linear FM PC waveform into two segments, one for the down sweep and the other for the upsweep. Note that the matched filter response can be obtained using the cross-correlation function xcorr(x, y), where x is the chirp signal and $y = x \cdot \exp(-j2\pi \cdot f_d \cdot \tau)$. Use a PC pulsewidth of 100 μs and a chirp frequency band of 50 kHz.

```
% Ambiguity Function for V-FM
% ----------------------------------------
% vfmamb.m

clear;clf;clc;

% Input Chirp Bandwidth and Pulsewidth

bw=5e4;      % Bandwidth - Hz
T= 1e-4;     % Pulsewidth - sec

%Input Time Points

N=128;

% Set Time Base

t=-T/2:T/(N-1):T/2;

% Sample Two-Segment Complex Chirp

if t<=0;
   s= exp(j*pi*bw*t.*t/T);
   else
     s= exp(-j*pi*bw*t.*t/T);end;

% Form Ambiguity Function

Bx=[];

for fd=-2*bw:bw/11:2*bw;
   y=s.*exp(-j*2*pi*fd*t);
   chi=abs(xcorr(s,y));
   Bx=[chi;Bx];
end;

%subplot(211),
mesh(Bx,[135 45]);
title(['Ambiguity Function for V-FM Waveform']);
xlabel('time');ylabel('frequency');
zlabel('amplitude');

%subplot(212);contour(Bx);
%title(['Contour Plot']);
%xlabel('time');ylabel('frequency');
```

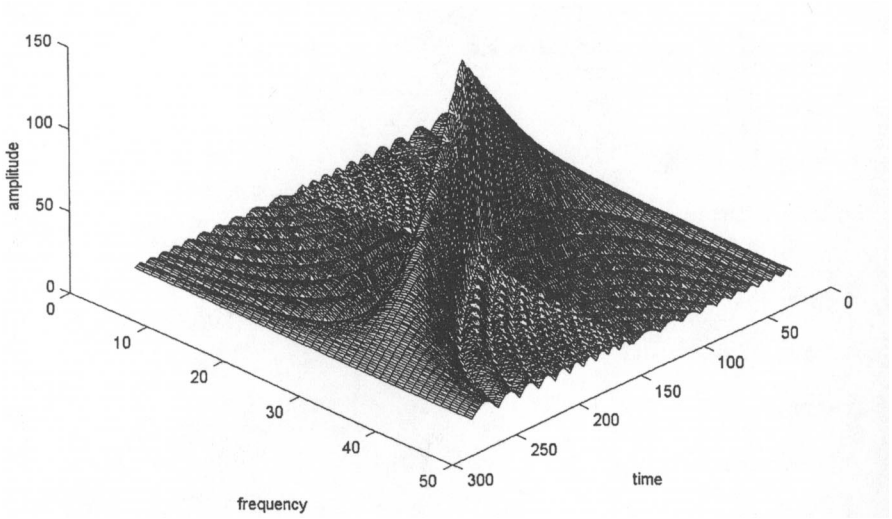

The ambiguity function for the linear-FM chirp shows that as the central frequency of the input signal is varied, the peak of the matched filter output varies in delay. Actually, the delay is a linear function of frequency. In the radar case, this range-Doppler coupling results in an apparent range shift with Doppler frequency that causes an erroneous range measurement. The actual target range may either lead or follow the apparent range depending upon whether the target Doppler is positive or negative.

The linear FM PC radar is more susceptible to repeater jamming than is a conventional radar. To see this, consider the ambiguity diagram depicted in Example 4.3. This diagram shows the output waveform of a PC radar for various mismatches in frequency. The output for the PC radar matched in frequency is shown along the central time axis of the diagram. By appropriately mismatching in frequency, the repeater jammer can generate a false target, which either leads or lags the occurrence of the matched target. Thus, this type of PC radar does not have the capability of a conventional radar to discriminate against a repeater jammer using leading-edge tracking. This makes it easier for a DECM to capture a PC radar than if a conventional waveform were employed.

Compressive ESM receivers also use linear FM PC techniques. The linear coupling of time delay with frequency allows the compressive receiver to separate multiple simultaneously occurring signals. This is equivalent to an instantaneous spectrum analysis of the signal set within a time window that corresponds to the shortest pulse width signal.

A block diagram of a digital system that accomplishes PC is depicted in Figure 4.1. Note that this system implements (4.4) using the FFT to find the

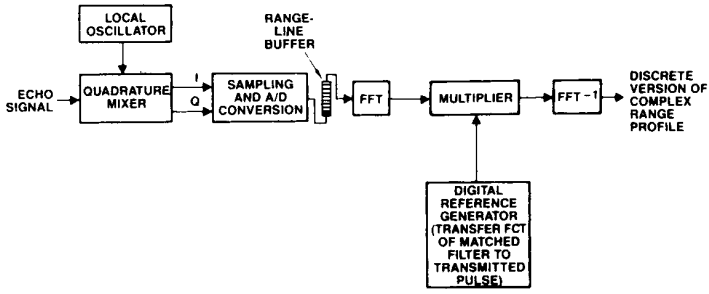

Figure 4.1 Digital PC. (*Source:* [15].)

Fourier transform of the signal and matched filter impulse response and the inverse FFT to convert the output signal back into the time domain.

In this method, a digitized version of the input signal at baseband (I and Q channels) is convolved with a digitized reference function that corresponds to the impulse response of the matched filter to the PC signal. This is accomplished in the frequency domain by first performing an FFT on the input signal, resulting in $V(\omega)$, which is then multiplied by the matched filter transfer function $V^*(\omega)$, thereby providing the PC output frequency spectrum $G(\omega) = V(\omega)\ V^*(\omega)$. This is then converted into the time domain by performing an inverse FFT on the output spectrum, resulting in $g(t) \leftrightarrow G(\omega)$. The advantage of this fully digital version is that large time-bandwidth product PC systems can be accomplished since the component limitations of analog implementations are bypassed.

4.1.2 Phase-Coded Pulse Compression

The most common form of this PC method uses binary phase coding. In this form of PC, a long pulse of duration T is divided into n segments each of width τ. The phase of each segment is chosen to be 0 or π in a pseudorandom manner. The time-bandwidth product of this PC signal is equal to the number of segments $n = T/\tau$. An advantage of this method is that a matched filter can be implemented using a simple tapped delay line (digital shift register) whose taps are spaced by the subsegment width τ and weighted by the phase (0 or π) corresponding to the appropriate sequence of random phases.

Barker code binary sequences are often used in phase-coded PC systems. These sequences have the property that the voltage time sidelobes are equal and have magnitude $1/n$. Unfortunately, the longest known Barker code has length 13 (1, 1, 1, 1, 1, −1, −1, 1, 1, −1, 1, −1, 1), where a 1 corresponds to 0 radians phase shift and −1 to π radians phase shift.

When larger PC ratios are desired, linear shift register sequences are often used. These sequences are generated using shift registers with feedback. An N-stage register can generate a maximal length sequence of $n = 2^N - 1$. For large sequences, the peak voltage sidelobes are approximately $1/\sqrt{n}$ while the time-bandwidth factor is n. The sequences computed in Example 4.4 are not unique. For example, for $N = 5$, there are a total of six maximal length sequences [5].

▶ *Example 4.4*

Using MATLAB, construct a general program that generates maximum length sequence codes using feedback shift registers. Plot the auto correlation function for a five-stage 31-bit sequence. What is the maximum time sidelobe?

Number of Stages	*Feedback Stage*
2	1, 2
3	2, 3
4	3, 4
5	3, 5
6	5, 6
7	6, 7
9	5, 9
10	7, 10
11	9, 11

```
% Binary Maximal Length Sequence Code
% Program Generates a Random Sequence
% ----------------------------------
% maxlen.m

clear;clc;

% Code Length and Feedback (m=2-7;9-11)

m=input('length=');
a=m-1;
if m==5;a=3;end;
if m==9;a=5;end;
if m==10;a=7;end;
if m==11;a=9;end;
l=2^m-1;

% Start sequence
```

```
x= eye(1,m);
z=x;

% Generate sequence of zero-ones

for j=1:l;
    for i=2:m;x(i)=z(i-1);x(1)=z(a)+z(m);end;
    if x(1)==2;x(1)=0;end;
y(j)=z(m);z=x;end;

% Convert to sequence of 1,-1

for i=1:l;
    if y(i)==0;y(i)=-1;end;
end;

% Plot correlation

t=1:2*l-1;zz=xcorr(y);
plot(t,abs(zz));grid;
xlabel('Time');
ylabel('Voltage Correlation');
title(['Binary Code Autocorrelation']);

% Display Sequence

b=input('Display Sequence Yes=1;No=0;  ');
if b==1;disp(y);end;

end


» maxlen
length=5
Display Sequence Yes=1; No=0; 1
 Columns 1 through 12

–1 –1 –1 –1 1 –1 –1 1 –1 1 1 –1

Columns 13 through 24

–1 1 1 1 1 1 –1 – 1 –1 1 1 –1

Columns 25 through 31

1 1 1 –1 1 –1 1

»
```

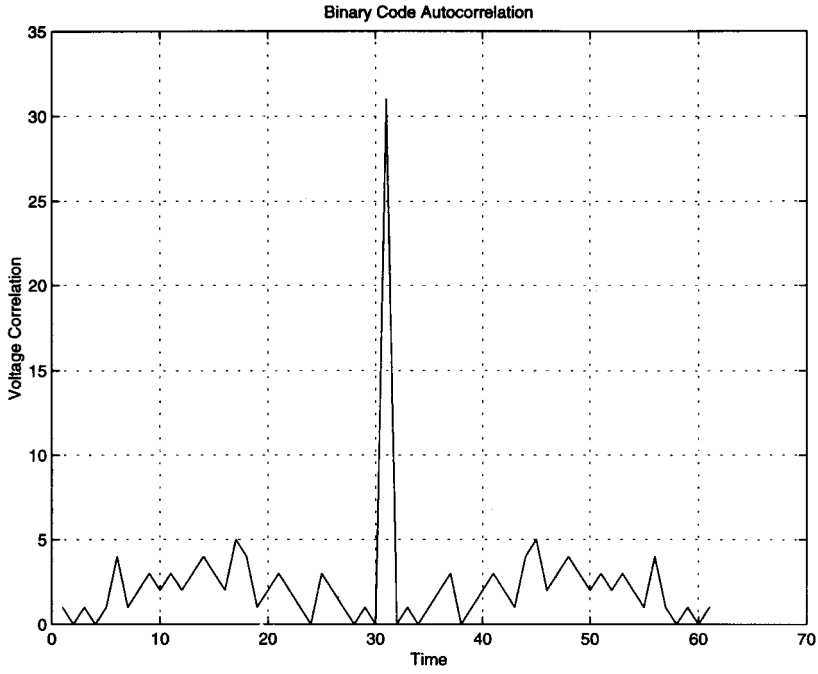

If Doppler processing is not required, the availability of different codes for phase-coded PC systems allows the coding to be changed on a pulse-to-pulse basis. This provides a counter to jammers that synthesize the PC waveform to generate false targets. However, DECM jammers that coherently repeat the intercepted waveform are still effective against this form of countermeasure.

Phase-coded PC waveforms are more sensitive than linear-FM waveforms with respect to Doppler frequency shift. Example 4.5 shows that for ratios of Doppler frequency to PC bandwidth as small as 0.05, significant distortion occurs in the compressed Barker-coded waveform and time sidelobes are much greater. Thus, phase-coded waveforms are not appropriate for radar that are designed to detect high-velocity targets. Also, EA jammers that synthesize phase-coded PC waveforms need accurate frequency set-on receivers to prevent dilution of the jamming signals and reduced effectiveness.

▶ *Example 4.5*

Using MATLAB, plot the matched filter output for a 13-bit Barker-coded PC waveform. Then replot the waveform for various ratios of Doppler frequency (f_d) shift to waveform bandwidth (B). Determine the f_d/B ratio where significant distortion occurs.

```
% Pulse Compression Mismatch
% -------------------------
% pcmissa.m

clear;clf;clc;

% Enter Barker code

xx=[1 1 1 1 1 -1 -1 1 1 -1 1 -1 1];

% Enter freqency offset fd/bw

r=[0 .02 .05 .07];
zz=[];

% Form input signal

for i=1:4;
rr=r(i);
dp=2*pi*rr;
  for n=1:13;
  y(n)=xx(n)*exp(j*n*dp);end;

% Form cross correlation

yy=xcorr(y,xx);
z=abs(yy);

if i==1;zz=z;
  elseif i>1;zz=[zz z];end;
end;

% Plot cross correlation

t=1:25;
subplot(221);
zx=zz(1:25);
plot(t,zx/max(zx)),grid;
title(['Barker Code Fequency Mismatch']);
axis([0 25 0 1]);
text(15,.9,['fd/bw=',num2str(r(1))]);

subplot(222);
zy=zz(26:50);
plot(t,zy/max(zy)),grid;
title(['Barker Code Frequency Mismatch']);
axis([0 25 0 1]);
text(15,.9,['fd/bw=',num2str(r(2))]);

subplot(223);
zw=zz(51:75);
```

```
plot(t,zw/max(zw)),grid;
title(['Barker Code Frequency Mismatch']);
axis([0 25 0 1]);
text(15,.9,['fd/bw=',num2str(r(3))]);

subplot(224);
zv=zz(76:100);
plot(t,zv/max(zv));grid;
title(['Barker Code Frequency Mismatch']);
axis([0 25 0 1]);
text(16,.9,['fd/bw=',num2str(r(4))]);
```

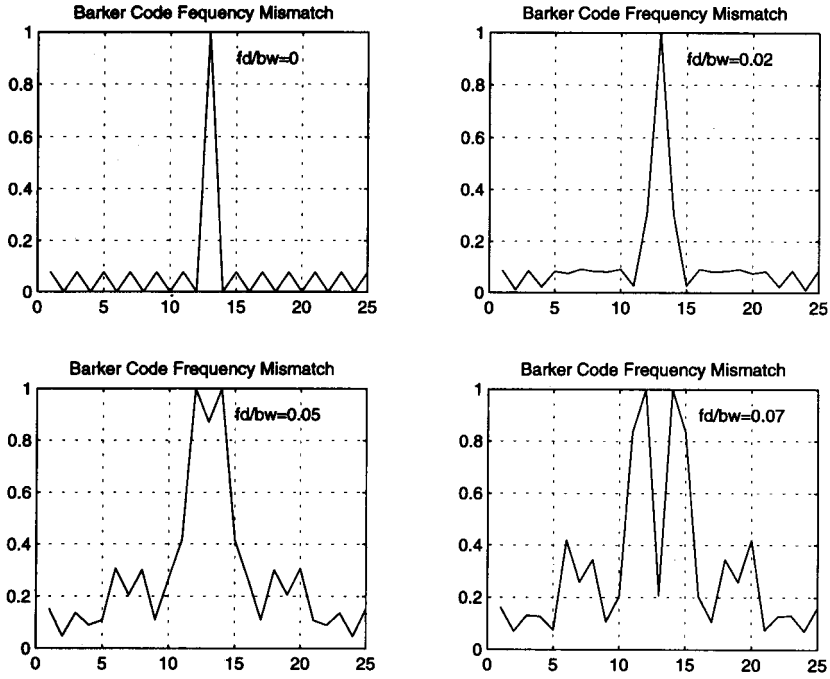

4.1.3 EA Against Pulse-Compression Radar

PC waveforms are commonly used in both surveillance and tracking radars. Jamming objectives depend on the type of radar to be jammed.

With surveillance radars, the object is generally to obscure the target by generating background interference or by synthesizing a false target that suppresses the detection of the true target. The latter procedure is sometimes called camouflage jamming.

For tracking radars, the objective is to generate a false target that captures the radar's tracking gates. The range-Doppler coupling properties of linear-

FM PC radar makes these radars vulnerable to repeater jammers. In this mode of operation, the radar's signal is coherently shifted in frequency and repeated back to the radar. The frequency-shifted repeater signal then leads the true target return of the output of the matched filter, making leading-edge tracking EP techniques ineffective.

Noise jamming is generally the most inefficient jamming waveform against PC radar. This can be examined by considering the PC system's matched filter as a correlator. Noise that is completely decorrelated with respect to the signal does not achieve any correlation gain while a target that is fully correlated achieves full processing gain. Jamming waveforms that achieve some degree of correlation are more effective than random noise.

CW signals generally produce some degree of correlation in the PC matched filter. For example, a CW waveform at the carrier frequency is correlated with a phase-coded waveform approximately half the time, achieving a 6-dB power gain with respect to a noise waveform. Also effective is coherently repeating half the PC waveform, thereby generating two false targets out of the matched filter that straddle the true target return.

▶ *Example 4.6*

Determine the effect of CW and noise jamming on a 31-bit maximal length sequence phase-coded PC signal. Assume the CW signal is at the carrier frequency so that it produces components in phase with the central frequency of the phase-coded waveform. Assume the noise is also at the central frequency but that it produces uniform phase modulation ($0 - \pi$) with respect to the phase-coded signal.

```
% Jamming of 31 Bit Shift Register Sequence
% With CW Noise
% ---------------------------------------
% cwjam.m

clear;clc;clg;

% Generate time vector

t=13/31*[1:1:61];

% Code order is 31-bit Maximal Length Sequence

x=[1 -1 1 1 -1 1 -1 1 -1 -1 1 1 1 1 -1 -1 -1 1 1 -1 ...
-1 1 -1 -1 -1 -1 -1 1 -1 1 1];

% CW-jamming in baseband with correct carrier
y=ones(1,31);

% Noise jamming in baseband with correct carrier
z=rand(1,31);
```

```
% Correlation of signal and jamming

acf1=xcorr(x);
acf2=xcorr(x,y);
acf3=xcorr(x,z);
effmv2=sum(acf2.*conj(acf2))/61;
effmv3=sum(acf3.*conj(acf3))/61;

% Plot jamming effects

subplot(211),plot(t,abs(acf1),':',t,abs(acf2));grid;
xlabel('Time in microsecs');
ylabel('Correlator Voltage Output');
title(['Pulse Compression Jamming With CW Jam Effect=', ...
num2str(effmv2)]);

subplot(212),plot(t,abs(acf1),':',t,abs(acf3));grid;
xlabel('Time in microsecs');
ylabel('Correlator Voltage Output');
title(['Pulse Compression Jamming with Noise Jam Effect=', ...
num2str(effmv3)]);
end
```

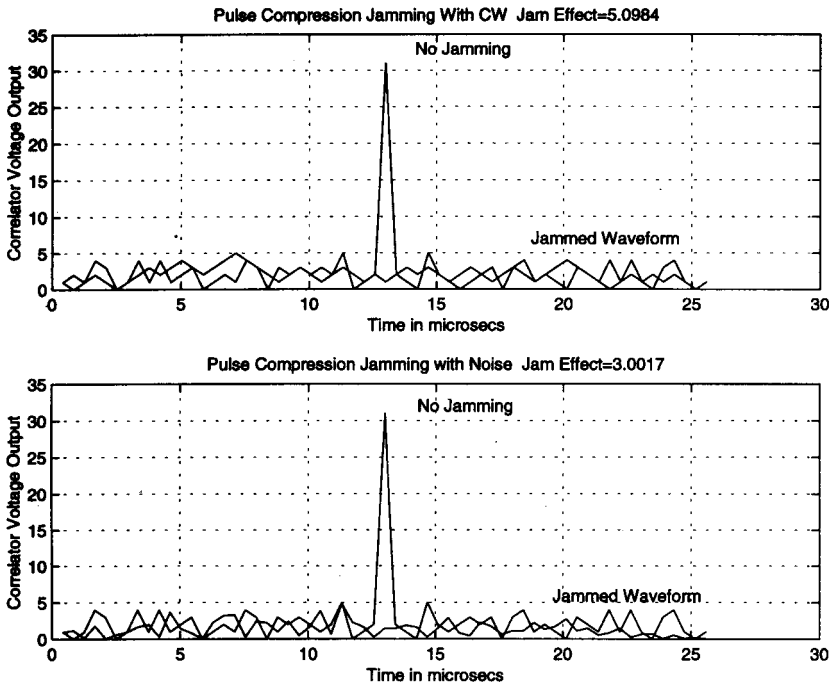

▶ *Example 4.7*

Determine the effect of half-code repeater jamming on a 31-bit maximal length sequence phase-coded PC signal. Use a combination of two 15-bit half codes plus one to fill the PC network.

```
% Pulse Compression Half Code Repeater Jamming
% ----------------------------------------
% pchalf.m

clear;clf;clc;

% Time Vector

t=13/31*[1:1:61];

% Maximal Length 31 Bit Sequential Code

x=[1 -1 1 1 -1 1 -1 1 -1 -1 1 1 1 1 -1 -1 -1 1 1 -1 ...
-1 1 -1 -1 -1 -1 -1 1 -1 1 1];

% Half Code Length

y=[1 -1 -1 1 1 1 1 -1 -1 -1 1 1 -1 -1 1];

% Jamming uses two halfs plus 1 to fill

z=[y y 1];

akf1=xcorr(x);
akf2=xcorr(x,z);

% Plot Jamming Effects

plot(t,abs(akf1),':',t,abs(akf2));grid;
xlabel('Time');ylabel('Correlator Voltage Output');
title(['Repeater Jamming with Half Pulses']);
text(14,30,'No Jamming');
text(18,14,'Repeater Jamming');
```

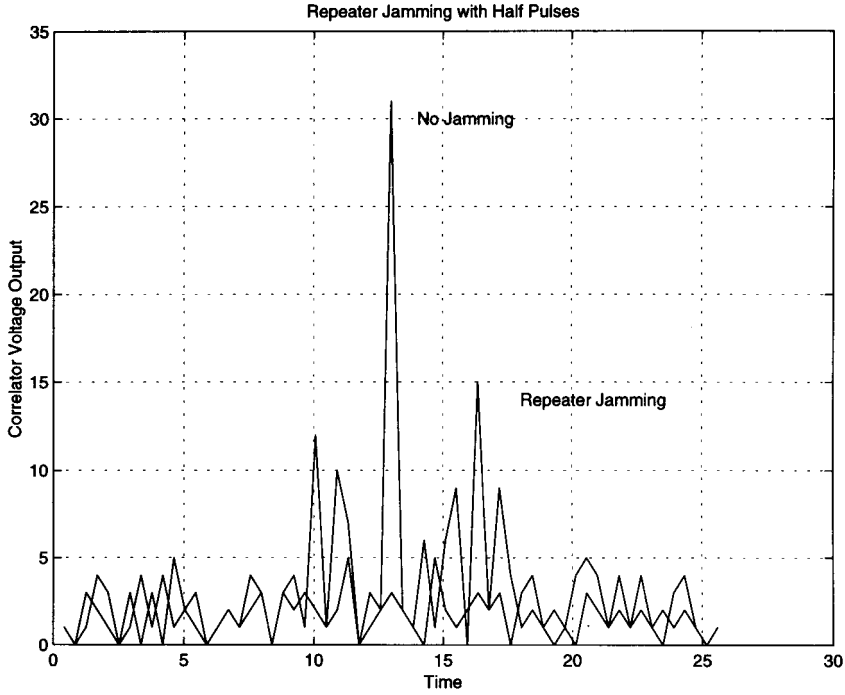

The first step in attacking a PC radar is to ascertain its parameters. There are two methods employed for this purpose. Older ES systems that employ envelope detectors destroy the phase (or frequency) information within the signal and hence rely on the fact that PC radars have long pulse widths for identification. Newer systems employ circuitry that measures the slope of the linear-FM chirp or the chip rate of phase-coded waveforms. These systems generally correlate the signal with a delayed replica in a phase detector to determine its phase properties similar to the *instantaneous frequency measurement* (IFM) receiver described in Section 6.3.

A block diagram of a general system to jam PC surveillance radars is depicted in Figure 4.2. This jamming system stores the input PC signal received from the radar in a *digital RF memory* (DRFM), where it is continually repeated and amplified throughout the radar's interpulse interval to create many false targets. Since the false jamming targets are coherent with the radar, they negate the processing gain of the PC network with respect to the radar target. Also, since they are synchronized with the radar's PRF, they receive the benefit of any post-detection integration performed by the radar.

In Figure 4.2, the DRFM can be replaced with a DDS to produce a similar effect. This is described in Section 5.4 and involves storage of the

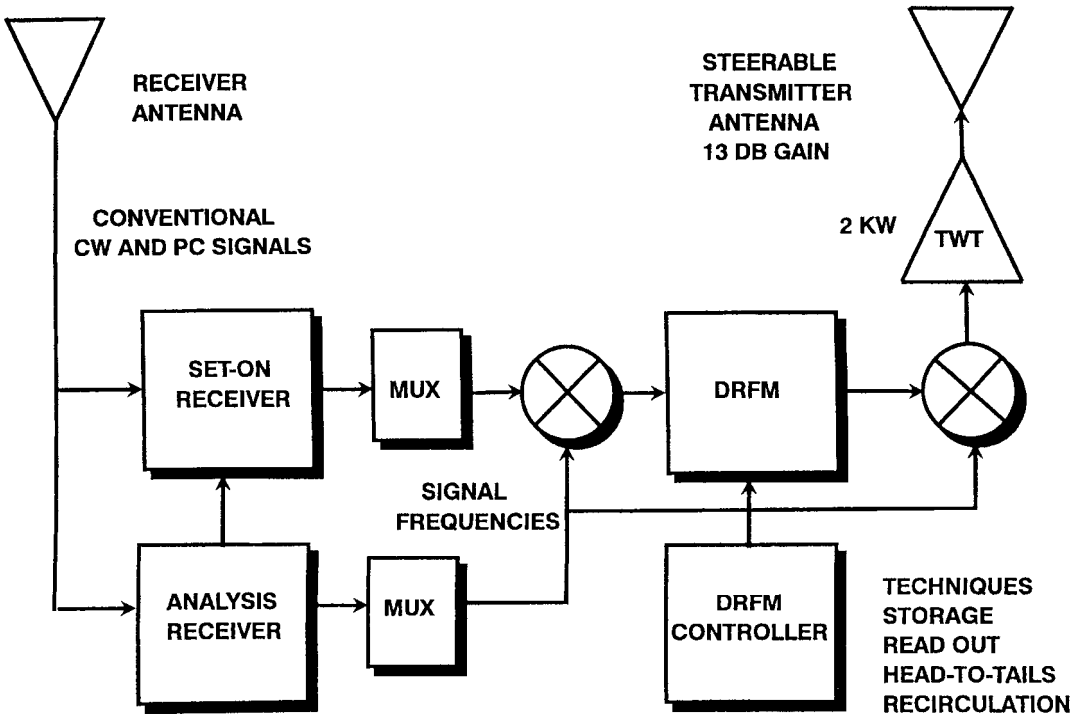

Figure 4.2 General PC jammer. (Skolnik, M., *Radar Handbook,* 2nd Ed., © 1990 McGraw Hill. Reprinted with permission.)

parameters associated with each threat radar in the jammer's library. The jammer receiver then identifies the particular PC radar to be countered, measures its critical parameters (i.e., such as the radar's frequency), draws its remaining parameters from the threat library, synthesizes a pseudocoherent replica of the threat radar's waveform in the DDS, and transmits this replica throughout the radar's interpulse interval. The effectiveness of the DDS approach depends upon how accurately the radar parameters are known or measured. As described in Section 3.5, frequency set-on is important for DDS-based jammers that counter phase-coded PC radar. This is a consequence of the rapid deterioration of the matched filter output of a phase-coded PC waveform with frequency off-set.

Repeater jamming against tracking radars using PC waveforms requires capture of the radar's tracking gates. To accomplish this, the DECM must repeat coherent replicas of the radar's PC waveform, possibly shifted in frequency, which can be varied with time. The procedure is to initially repeat the received radar pulse with minimum time delay. This ensures that the jammer pulse enters the radar's tracking gates along with the true signal and allows capture of the radar's *automatic gain control* (AGC) circuits. Then the DECM begins to introduce increasing amounts of time delay in the repeated signal. The range-gate circuitry in the radar begins to track the stronger jammer signal and gradually "walks-off" from the true target range.

Most tracking radars include two *electronic protection* (EP) devices against repeater jammers. They generally employ leading-edge range tracking that functions against just the leading edge of the received signal. Hence, DECM signals that initially include significant delay (i.e., greater than 20 ns to 50 ns) lag with respect to the true signal are rejected in favor of the true signal. In addition, tracking radars perform radial velocity checks by comparing the radial velocity derived from the received Doppler with that obtained by differentiating tracking range data. Hence, repeaters must induce realistic frequency shifts onto the repeated signal that are consistent with the range "walk-off" program. Also, some tracking radars differentiate Doppler to obtain a measure of the acceleration characteristics of the target. If this does not check with that of realistic targets, then the signal is rejected.

A block diagram of a repeater jammer using fiber optic delay lines is depicted in Figure 4.3. In this system, the RF input signal modulates a laser. The laser signals excite various lengths of monomode fiber optic cable that are interconnected using optical switches. The laser signal is demodulated using a photo optical diode to recover the RF signal. The delays available from the fiber optic coils are generally related in a binary manner. For example, if the shortest coil is 0.1 μs. in length, and eight coils are used, the delay available from the longest coil is 12.8 μs. Using this technique, the delay can be switched

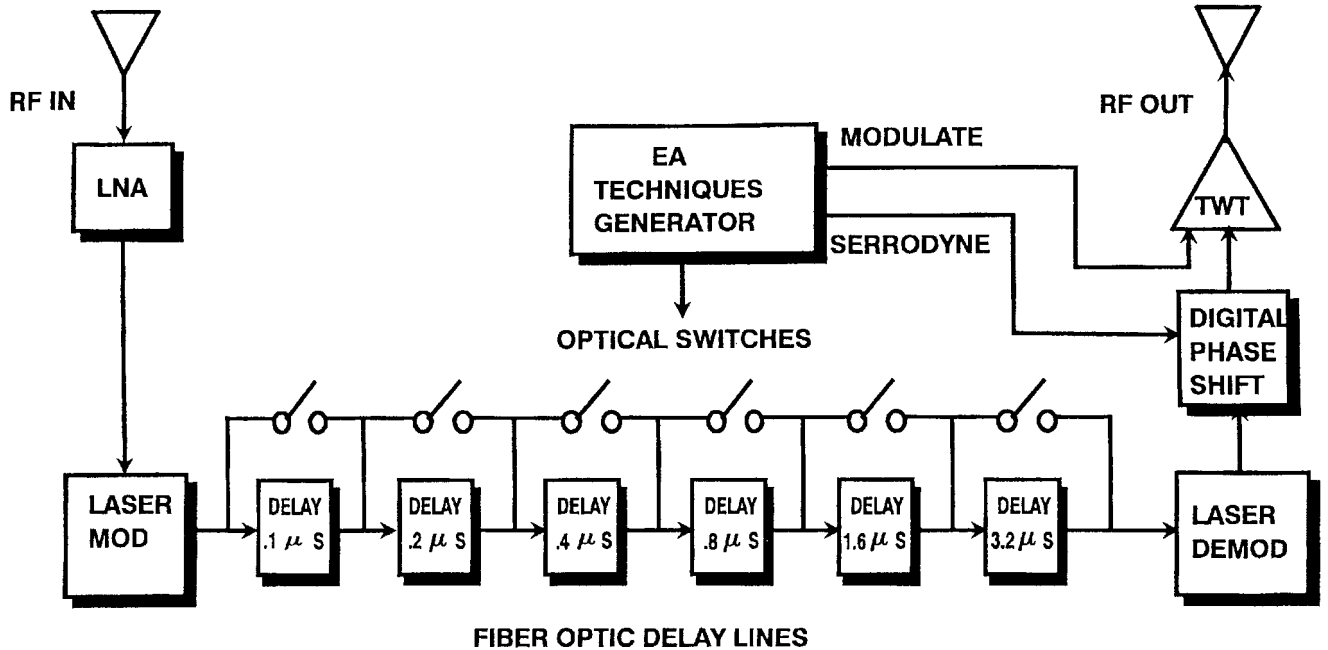

Figure 4.3 Repeater jammer using fiber optic delay lines.

in 0.1-μs steps to a maximum delay of 25.5 μs. With this method, a dynamic range of approximately 35 dB with 2-GHz instantaneous bandwidth can be achieved.

The simulation of Doppler shift in the previously described repeater jammer can be accomplished using mixers to down-convert and up-convert signals before and after propagation through the optical delay lines. The frequency offset between the down- and up-converted signals then represents the differential Doppler shift imparted onto the signal. A Doppler shift can also be imparted onto the jamming signal using a digital phase shifter as described in Section 3.3.2.

Alternately, a DRFM can be used to store PC signals in a DECM repeater jammer. With this method, input signals are converted to digital form by sampling at or above the Nyquist rate and stored in a digital memory. They are then clocked out when needed (minimum delay is the order of 10 ns to 20 ns) and converted to analog form for transmission. Practical implementation of DRFMs involves down-converting signals to baseband where they can be efficiently stored digitally. Doppler shifts can be imparted onto the signal by an appropriate frequency difference between down-conversion and up-conversion oscillator frequencies.

Storage of PC waveforms imposes some restrictions on DRFMs. This occurs because digital memory capacity for high clock speeds is limited. To accommodate long PC signals, the waveform is strobed and short durations of the complete signal are stored. When strobed, the short durations of stored signal are read out on a head-to-tails basis, thus creating a step-approximation to the whole waveform. For a linear-FM PC signal, the step approximations are smoothed in the radar's PC network. With phase-coded waveforms, the approximation is performed at the chip rate providing good resemblance to the real waveform. However, in this case, some phase discontinuities may exist at code transitions.

▶ *Example 4.8*

Using MatLab, plot the output of a linear-FM PC matched filter to signals with frequency offset. What offset frequencies produce output signals that lead or lag the signal with no frequency offset? Why is this effect useful in negating leading edge range trackers?

```
% PULSE COMPRESSION WAVEFORM WITH FREQUENCY OFFSET
% ------------------------------------------------
% pcoff.m

clear;clf;clc;
```

```
% Input Chirp Bandwidth,Pulsewidth and Offset Frequency

bw=1e6;    % Bandwidth - Hz
T= 1e-4;   % Pulsewidth - sec
fo=2e5;    % Frequency Offset - Hz

%Input FFT Points

lfft=1024;

% Set Time Base

t=-T/2:T/(lfft-1):T/2;

% Sample Complex Chirp

s= exp(-j*pi*bw*t.*t/T);

% Find Fourier Spectrum of Chirp

ZY= fft(s,lfft);
Y=fftshift(ZY);

% Find Chirp Power Spectral Density

Psd=Y.*conj(Y)/lfft;
A=ceil(max(Psd));
l=length(Y);
f=(1/T)*(-(l-1)/2:(l-1)/2);

% Find Matched Filter Chirp Time Waveform

zh=ifft(Psd,lfft);
h=fftshift(zh);

% Input Frequency Offset Signals

s1=exp(-j*2*pi*fo*t)+exp(j*2*pi*fo*t);
so=s.*s1;

% Find Fourier Spectrum of Offset

ZZY=fft(so,lfft);
YY=fftshift(ZZY);

% Find Power Spectral Density of Offset

Psd1=YY.*conj(Y)/lfft;

% Find Offset Matched Filter Time Waveform

zzh=ifft(Psd1,lfft);
hh=fftshift(zzh);

% Plot Time Waveform
```

```
plot(t,abs(h),t,abs(hh));grid;
axis([-T/4 T/4 0 1 ]);
title(['PC Matched Filter Output']);
xlabel('Time - Sec');ylabel('Amplitude');
text(.2e-5,.95,'No Offset');
text(-2.4e-5,.85,'Repeater With Offset Frequency');
text(.4e-5,.85,'Repeater With Offset Frequency');
```

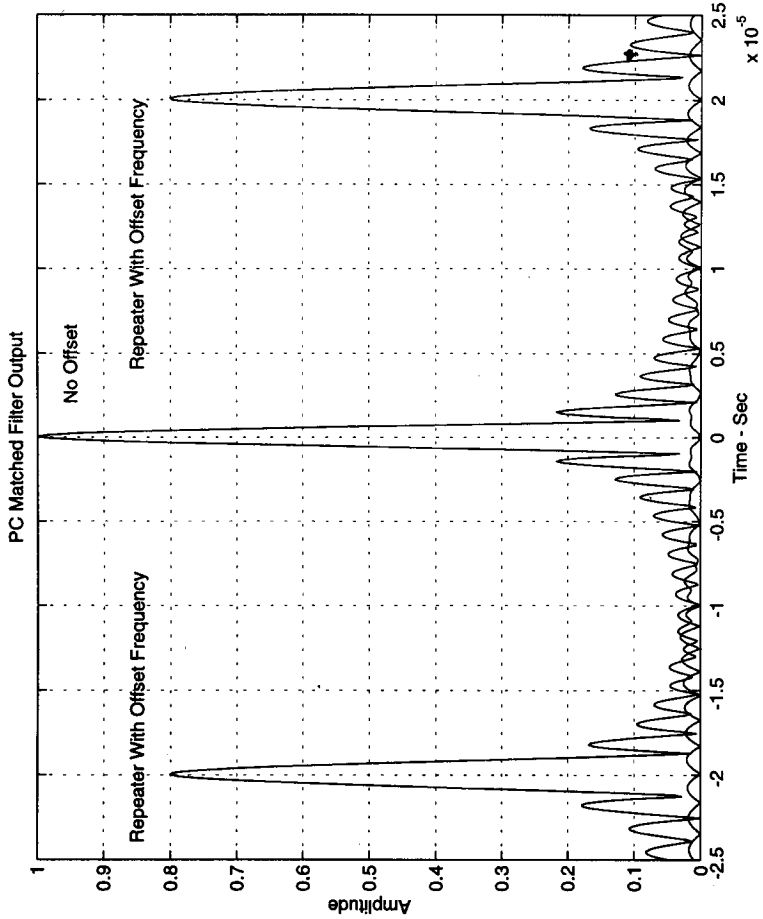

4.2 Pulsed Doppler Radar

With the rapid advance of digital signal processing and stable microwave power sources, the use of PD radars has dominated the modern radar field, particularly in airborne radar applications. These radars use the Doppler effect to extract targets from background interference on the basis of their velocity signature, providing modern airborne radars with "look-down–shoot-down" capability.

The magnitude of the Doppler shift frequency can be computed by noting that the phase of the return from a scatterer, when received at the radar, is given by $\phi = 4\pi r/\lambda$ radians, where r is the range to the scatterer and λ is the radar's apparent wavelength. The Doppler shift can then be found as

$$f_d = \frac{1}{2\pi}\frac{d\phi}{dt} = \frac{2v_r}{\lambda} \tag{4.13}$$

where v_r is the target's radial velocity. This result is accurate except for high-velocity targets where a correction factor $2 \cdot (v_r/c)^2 \cdot f_t$ applies.

► *Example 4.9*

For an airborne radar, plot the constant Doppler contours on the ground, called "isodops," as a function of the ratio v_g/v_{ac}, which varies from 0 to 0.9 in 0.1 increments, where v_g is the Doppler velocity on the ground and v_{ac} is the aircraft's velocity. How would you use this plot to determine the frequency spectrum of ground clutter?

```
% PLOT OF CONSTANT DOPPLER CONTOURS - ISODOPS
% ------------------------------------------
% isodop.m

clear;clc;clf;

% Set Aircraft Parameters

ro=.1;                % vg/vac ratio
h=10000;              % feet

% Calculate Doppler Contour

for i=1:9;
rr=ro+.1*(i-1);
phi=acos(rr);         % depression angle
a=tan(phi);
xmin=h/a+1e-3;
x=xmin:30000;
y1=sqrt(a^2*x.^2-h^2);
q=1:xmin;
Ay=zeros(size(q));
Ay1=[Ay y1];
```

```
% Plot Doppler Contour

Ax=xmin*ones(size(q));
x1=[Ax x];
plot(x1,Ay1,'k',x1,-Ay1,'k',-x1,Ay1,'k',-x1,-Ay1,'k');
grid;axis([-3e4 3e4 -5e4 5e4]);hold on;
end;hold off;
title('Constant Doppler Contours - Isodops');
xlabel('Ground Track Range - feet');
ylabel('Cross Track Range - feet');
text(2.5e4,.2e4,'Ground Track');
```

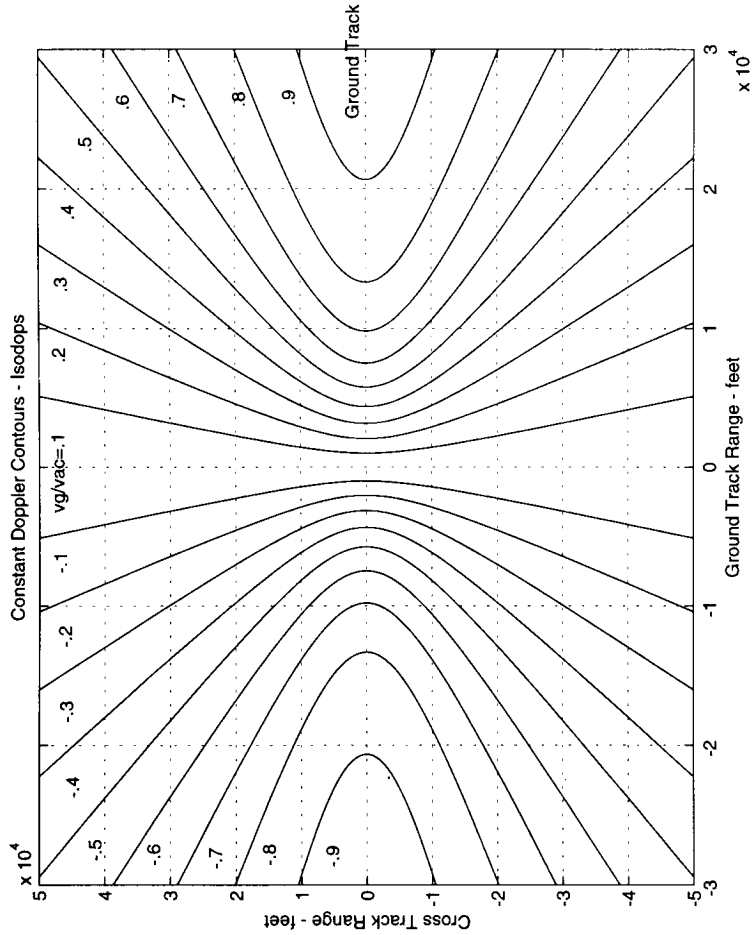

A block diagram of a simple pulse Doppler radar is depicted in Figure 4.4 [13]. The transmitter generates a train of phase stable pulses at a particular PRF. The signals returned from the target illuminated by a PD radar are generally processed in a set of narrowband filters that coherently integrate the signals to which they are tuned. The filters both resolve and enhance signals within a particular velocity band. In search radar applications, the bank of contiguous Doppler filters is used to cover the velocity band of interest to extract specific targets and reject clutter and targets outside that velocity band. Once the target is acquired, only one filter may be needed for tracking. In tracking radar applications, such as missile seekers, a speed gate may be used that basically consists of a narrowband Doppler filter that is caused to follow the targets Doppler using a servo technique.

The bandwidth (B_d) of a Doppler filter is inversely proportional to the time in which a signal is processed within the filter which is called the *coherent processing interval* (CPI). For search radar, the CPI must be shorter than the time (T_d) the antenna dwells on the target. The number of pulses coherently integrated is given by CPI · PRF, resulting in a processing gain with respect to noise of

$$PG = 10 \log(CPI \cdot PRF) \tag{4.14}$$

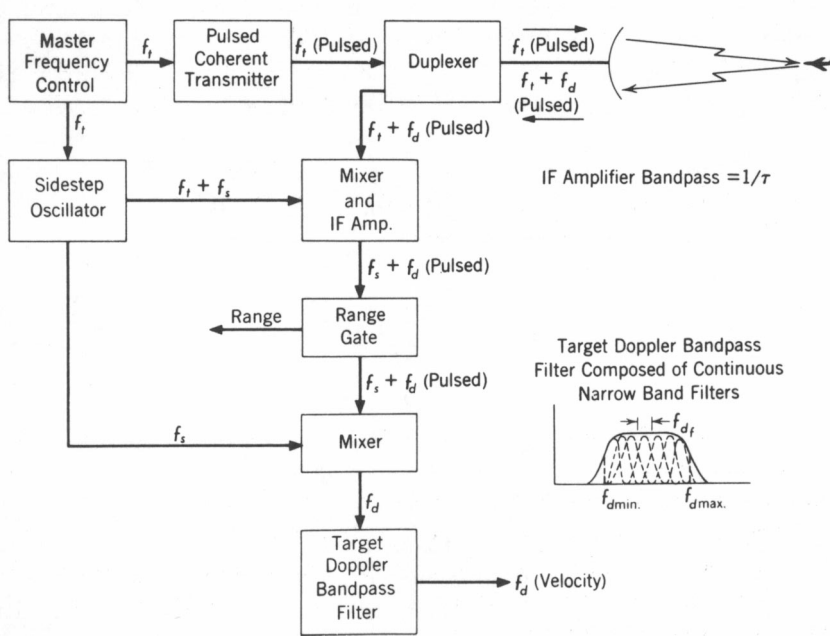

Figure 4.4 Block diagram of pulsed Doppler radar. (*Source:* [13].)

Using mixed predetection (coherent) and postdetection integration (matched to T_d), it is possible to provide good overall detection performance for the PD radar while changing the transmitted frequency or *pulse repetition frequency* (PRF) on a block-to-block (i.e., CPI) basis. The block-to-block frequency changes are useful in applying frequency agility to the PD radar and PRF changes are useful in resolving range ambiguities.

As an example, consider a ground-surveillance PD radar that rotates at 36 degrees/s, has an azimuth beam width of 3.6 degrees, and a PRF of 50 kHz. The dwell time of this radar is 3.6 degrees/(36 degrees/s) or 100 ms. If the CPI for this radar is set equal to the dwell time, then the Doppler filter bandwidth is 10 Hz while the processing gain is 5000 or 37 dB. From an EA standpoint, when noise jamming is used, this processing gain must be compensated by employing additional jamming ERP. When deceptive jamming is used, the deceptive jamming signal must be highly accurate in frequency so that it can compete with the true signal within the Doppler filter's 10-Hz bandwidth.

The preceding example illustrates how employing interpulse coherence makes the PD radar very difficult to jam unless the jammer system employs equivalent coherence. This has resulted in the emergence of the DRFM as a primary component in EA systems against PD radar.

PD radars can be categorized as low, medium, or high PRF, according to whether Doppler (low PRF), range (high PRF), or range and Doppler (medium PRF) are ambiguous. From an EA viewpoint, it is important to understand these PD modes since each presents different jamming opportunities.

Unambiguous range (nmi) in a radar is given by $R_u = 80.91/\text{PRF (kHz)}$, while unambiguous velocity (knots) is given by $v_u = 971 \cdot \lambda\text{(m)} \cdot \text{PRF (kHz)}$, resulting in

$$R_u v_u = \frac{2.3565 \cdot 10^4}{f_{\text{GHz}}} \tag{4.15}$$

Equation (4.15) illustrates that it becomes more difficult to achieve unambiguous range and velocity as the frequency of the radar is increased. For example, if the radar must detect targets with unambiguous velocities as high as 600 knots, then at a frequency of 1 GHz the unambiguous range is 40 nmi. If the frequency is raised to 10 GHz, then the unambiguous range is reduced to 4 nmi. Further, for an airborne radar, the appropriate velocity to consider is the closing velocity between the radar and the target (i.e., 1200 knots for a 600-knot platform velocity), which compounds the problem.

▶ *Example 4.10*

Using the expression for range-velocity ambiguities given in (4.15), plot a curve of unambiguous velocity versus unambiguous range using frequency as a parameter.

```
% Unambiguous Range-Velocity Chart
% --------------------------------
% unamb.m

clf;clc;clear;

% Define Range Vector

Rmin=3;    % Nmi
Rmax=1000; % Nmi
R=Rmin:Rmax;

% Define Frequency Values

f=[.1 .3 .6 1 3 6 10 16 35 60]; % Ghz

% Compute Unambiguous Velocity

for k=1:10;
v=2.3565e4./(R*f(k));
vr(:,k)=v';
end;

% Plot Unambiguous Range/Velocity

loglog(R,vr,'k');grid;
xlabel('Unambiguous Range - nmi');
ylabel('Unambiguous Velocity - knots');
title(['Unambiguous Range - Velocity']);
axis([ 5 1000 10 3000 ]);
```

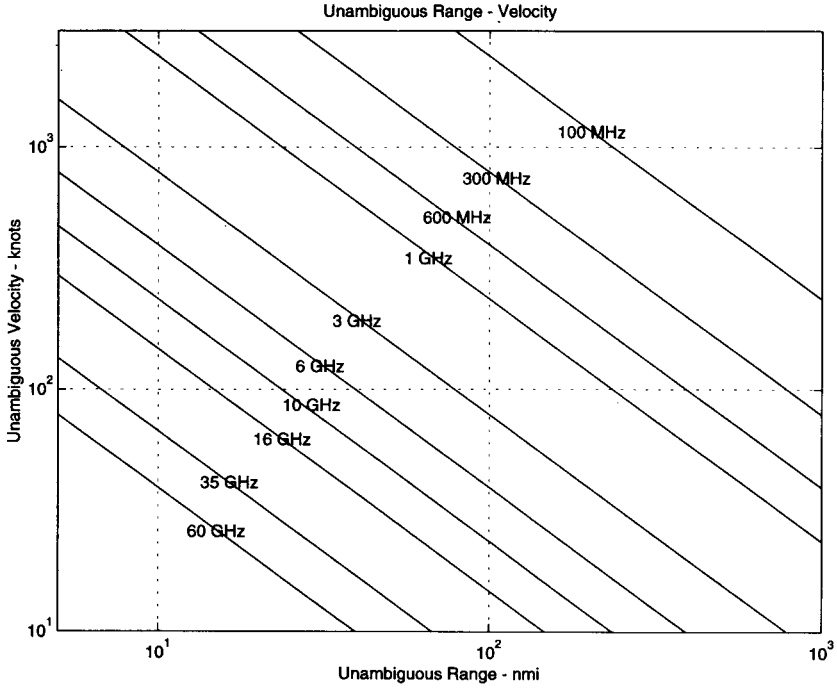

Figure 4.5 depicts the three PRF types in range-Doppler space for an *airborne intercept* (AI) application. In general, the interpulse period is divided into range cells (range gates) that correspond to the radar's transmitted bandwidth (τ_e = 1/BW), and the Doppler space is divided into Doppler cells (Doppler filters), the bandwidth of which is inversely proportional to the dwell time of the radar antenna's mainbeam on the target. The number of range gates is greatest for a low-PRF radar, whereas only a small number is used for a high-PRF radar. Conversely, only a small number of Doppler filters is used in a low-PRF design, whereas a large number are used in a high-PRF design. Although the interpulse period is generally filled with range gates for all types, the low-PRF type is the only design that fills the frequency region between PRF lines with Doppler filters. In medium-PRF designs, those Doppler frequencies occupied by ground vehicular traffic are generally excluded from the Doppler frequency coverage region. Generally, the high-PRF design fills only the Doppler-clear region ($2v_r/\lambda < f_d < PRF - 2v_r/\lambda$) with Doppler filters, whereas the medium-PRF design excludes the region occupied by moving vehicular targets from the Doppler coverage.

The principal advantage of a low-PRF design is its ability to restrict clutter intake to just that which is in the same range cell as the target. For

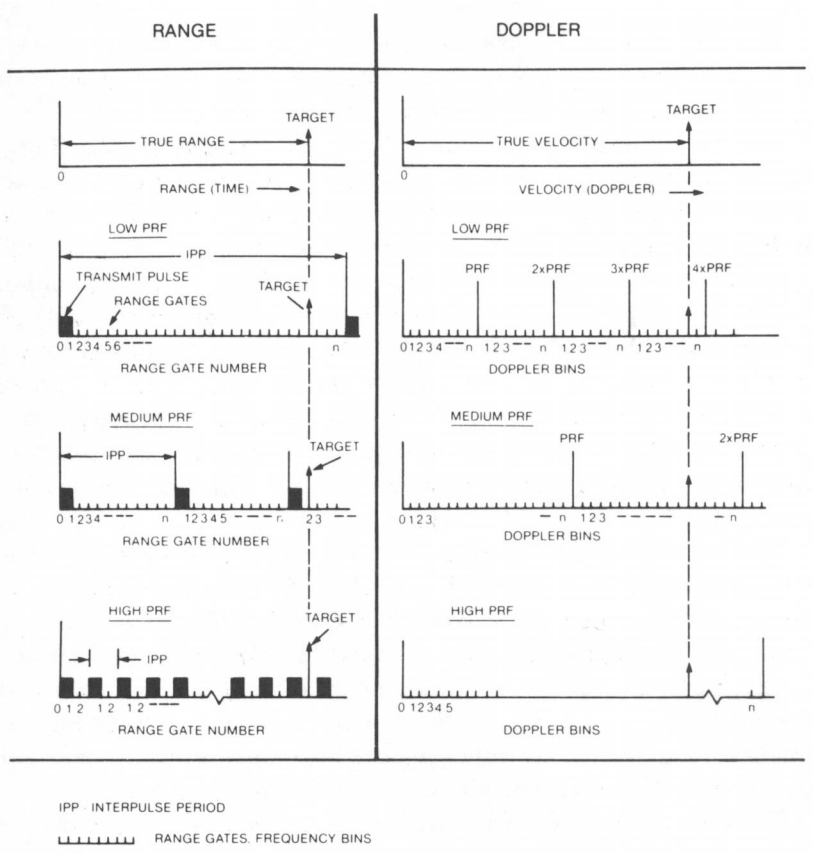

Figure 4.5 Pulsed Doppler radar in range-Doppler space. (*Source:* [16].)

example, a rain or chaff clutter cell several miles in extent would not interfere with targets not directly in the cell, whereas, in a medium- or high-PRF design, this same rain cell could clutter the entire unambiguous range interval. Also, sidelobe and main-lobe clutter can be restricted by increasing the range resolution of the radar and are not magnified by folding ambiguous clutter returns from short range into the same range cell as the target.

Other features of the low-PRF design include the ability to use a *sensitivity-time-control* (STC) function that allows normalization of the clutter return over the full range of the radar and the fact that range can be directly measured without generating any spurious targets. STC cannot be used in medium- or high-PRF designs because it would attenuate long-range targets of interest as well as near-range clutter. This results in a low-PRF system processor requiring less dynamic range, which allows better control of false alarms. In medium-

and high-PRF designs, a range correlation system is required to resolve the resulting ambiguous ranges. When multiple targets are present, they can confuse the range correlator and generate spurious targets called *ghosts.*

On the negative side, in a low-PRF design, unless main-lobe clutter is separated in range from the targets the radar encounters, it can be rejected only on the basis of differences in Doppler frequency. The highly ambiguous Doppler response causes a lack of Doppler visibility, requiring the use of staggered or randomly jittered PRF to eliminate blind velocity zones. In airborne radars, the frequency of the mainbeam ground clutter is generally translated to zero frequency. The spread of the main-lobe clutter spectrum is then determined primarily by the aircraft's velocity, azimuth antenna beamwidth, and azimuth look angle. At azimuth angles significantly off the aircraft's ground track (i.e., 30 degrees to 90 degrees), the main-lobe spectrum generally occupies a large fraction of the frequency region between PRF lines. The wide Doppler notch blinds the low-PRF airborne PD radar to many targets of interest.

The use of high-PRF radar is most prevalent in airborne applications where targets are closing on the radar. The high-PRF radar allows the average transmitter power to be maximized by increasing the PRF. At I-band, typical PRFs for airborne radar are the order of 100 kHz to 300 kHz with duty factors as high as 50%. To achieve the same amount of average power with a low-PRF radar, subject to a transmitter peak power limitation, requires increasing the radar's pulse width and employing large amounts of PC to provide the degree of range resolution essential to low-PRF radar operation.

A feature of the high-PRF waveform in an airborne application is that slow-moving ground-based targets can be eliminated because such a wide Doppler spectrum is available for target processing. For example, in an X-band high-speed interceptor (i.e., ground speed equal to 1500 knots), the sidelobe clutter spectrum will extend out to 50 kHz. If the expected targets close on the interceptor at a maximum of 600 knots, then an additional 20 kHz of clear Doppler must be provided. If a PRF of 150 kHz, for example, is selected, the lower zone of 80 to 100 knots can be discarded to eliminate ground targets. The result would have only minimal effect in the detection of high-speed closing aircraft targets.

High-PRF airborne radar designs generally operate in a velocity-only search detection mode for initial detection. In this mode, range ambiguities are not resolved and a maximum detection range equivalent to that of a CW radar (i.e., with an average power of $P_A = P_p d_u$) is achieved. When range information is desired, the high-PRF design must employ frequency modulation of the RF carrier (e.g., linear or sinusoidal frequency modulation) or multiple PRFs during the radar's dwell time on target to resolve the range. This require-

ment may cause an estimated 20% to 25% degradation in detection range compared to that achieved when range information is not required. A significant limitation of the high-PRF waveform for airborne applications is its limited ability to detect targets moving at velocities that cause their Doppler frequencies to appear in the sidelobe clutter regions. The clutter-free detection regions occur in the forward or closing aspects of the target; whereas for rear or chasing aspects, the target must compete with large sidelobe clutter returns, particularly at low altitudes.

With the high-PRF waveform, range folding causes short-range clutter to compete with long-range targets. In particular, all the sidelobe clutter folds into a small ambiguous range interval due to the many range ambiguities. For example, with a PRF of 150 kHz, the unambiguous range is only 0.5 nmi and, because sidelobe clutter can be well above receiver noise out to beyond a range of 10-nmi, more than 19 ambiguities of clutter will be folded into the PRF interval. Hence, at low altitudes, sidelobe clutter generally will obscure targets located within its velocity domain (i.e., $f_d = \pm 2v_r/\lambda$).

In summary, a high-PRF waveform provides ghost-free target Doppler, the capability to reject slow-moving targets, and a clutter-free target detection region that generally facilitates detection of closing targets. However, the limited all-target aspect detection, especially at low altitudes in tail chases, generally restricts the use of this waveform to closing targets. In addition, high-PRF designs require complicated methods for resolving range ambiguities and may also suffer from eclipsing problems, where target returns are lost, either totally or partially, because the receiver is blanked when the target is received due to the high duty factor of the waveform.

Medium-PRF airborne radar was conceived as a solution to the problems of detecting tail-aspect targets in the presence of both main-lobe and strong sidelobe clutter, thereby providing good overall coverage from all aspects. For modest operating ranges, the PRF can be set high enough to provide adequate separation between the periodic repetitions of the main-lobe clutter spectrum without incurring particularly severe range ambiguities. Main-lobe clutter can then be rejected through Doppler filtering, and individual targets can be extracted from sidelobe clutter using a combination of Doppler filtering and range resolution discrimination. Also, ground moving targets, being similar in characteristic to mainlobe clutter, can be rejected using a medium-PRF design.

The key feature of medium-PRF airborne radar operation is its ability to detect tail-aspect moving targets in a sidelobe clutter background. Increasing the PRF over low-PRF operation opens the clear region between mainlobe clutter responses that occur at multiples of the radar's PRF. This makes it easier to construct practical Doppler filters to both reject main-lobe clutter

and bracket the target's response, thereby rejecting that sidelobe clutter not in the target's Doppler resolution cell (e.g., $B_D = 1/T_d$, where T_d is the time on target).

However, in the process of increasing the PRF, range ambiguities are created that allow close-in main-lobe and sidelobe clutter to enter the range resolution cell containing the target. Main-lobe clutter can be rejected through the use of a comb filter (e.g., MTI canceller) just as for a low-PRF design except that the rejection capability must be increased due to the ambiguous clutter. Sidelobe clutter must be rejected through increased Doppler resolution (e.g., bandpass filtering), which serves the dual function of attenuating the clutter outside the target's Doppler resolution cell while minimizing the unavoidable sidelobe clutter intake within the Doppler filter containing the target. A prime consideration in the design of medium-PRF radar involves the minimization of the unavoidable sidelobe clutter intake that ultimately limits the radar's performance.

The clutter intake into a medium-PRF airborne radar is regulated through sorting by both range and Doppler frequency. Sorting by range is accomplished using range gates that isolate the returns received from relatively narrow strips of ground at constant range. Because of the range ambiguities, the return passed by each gate will come from several strips of grounds.

Sorting sidelobe clutter by Doppler frequency is accomplished by applying the output of each range gate to a bank of Doppler filters. They will isolate the returns received from strips of ground lying between lines of constant angle relative to the radar's velocity, which are called *isodops* (see Example 4.9). Because of Doppler ambiguities, any one filter will pass the returns from several strips.

The medium-PRF waveform combines some of the attributes of both high- and low-PRF waveforms, which for airborne applications can provide slow-moving target rejection, all-target-aspect coverage, sidelobe clutterfree regions, and accurate range information. The range and Doppler ambiguities of a medium-PRF design cause the returns from short-range sidelobe clutter to fold into the same Doppler regions occupied by target returns. However, the essence of medium-PRF waveform design is to establish clear regions within the range-Doppler space by the judicious placement of multiple medium PRFs.

To resolve both range and Doppler blind zones occurring in medium-PRF airborne radar, the radar's PRF is cycled through a fixed number of fairly widely spaced PRFs while the radar's main lobe dwells on the target. For example, the radar might be cycled through eight different PRFs. If a target is in the clear on any three PRFs and its echoes exceed the detection threshold on all three, the target will be deemed detected. The range ambiguities and all spurious target ranges will then be resolved. The optimum PRF code is a

function of the operational situation such as radar altitude, clutter levels, and speeds that must be determined for each specific radar.

For a target to be detected during a particular transmitted PRF of a medium-PRF code, it must be simultaneously in both a Doppler-clear region and in a range-clear zone. If the target's Doppler frequency falls in a Doppler blind zone, its return will not pass through a Doppler filter and be detected, despite the fact that it is in a range-clear zone. If the target is in a range blind zone, although its return may pass through a Doppler filter, it still will not be detected because the accompanying sidelobe clutter through the filter will cause the detection threshold to be greater than the target response. Figure 4.6 depicts a range-Doppler matrix of a representative medium-PRF radar that shows the zones for which the radar is both range-clear and Doppler-clear for at least three of eight widely spaced PRFs. Note that for a tracking radar, the PRF can be adaptively controlled to place the target in clear range and velocity zones so that only one burst at this PRF need be transmitted rather than the long, diverse bursts required by a search radar.

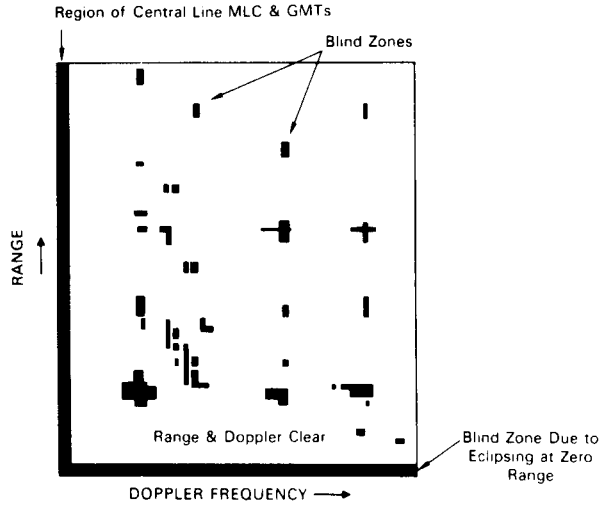

Figure 4.6 Range-Doppler regions in a medium PRF radar that are clear on at least three of eight PRFs. (*Source:* [17].)

► *Example 4.11*

Using MATLAB, plot the ambiguity diagram for a pulsed Doppler radar. Consider an eight-pulse burst and plot time for ±4 PRI intervals and frequency for ±2 PRFs.

```
% Ambiguity Function for Pulsed Doppler Waveform
% ----------------------------------------------
% ambfunb.m

clc;clf;clear;

N=2048;j=sqrt(-1);

% Waveform Parameters

Tp=1e-6;     % pulse width - sec
T=10e-6;     % period - sec
f=2e7;       % carrier frequency - Hz
Tx=8*T;      % burst length - sec

% Set Time Sampling

t=-Tx/2:Tx/(N-1):Tx/2;

% Sample Coherent Burst Signal

df=100*Tp/T;
zz=(1+square(2*pi*t/T,df))/2;
x=zz.*exp(j*2*pi*f*t);

% Form Ambiguity Function

Bx=[];

fr=1/T;
for fd=-2*fr:fr/11:2*fr;
  y=x.*exp(-j*2*pi*fd*t);
  chi=abs(xcorr(x,y));
  Bx=[chi;Bx];
end;

%subplot(211),
mesh(Bx,[-37.5 30]);
title(['Ambiguity Function for Pulse Doppler Waveform']);
xlabel('time');ylabel('frequency');
zlabel('amplitude');

%subplot(212);contour(Bx);
%title(['Contour Plot']);
%xlabel('time');ylabel('frequency');
```

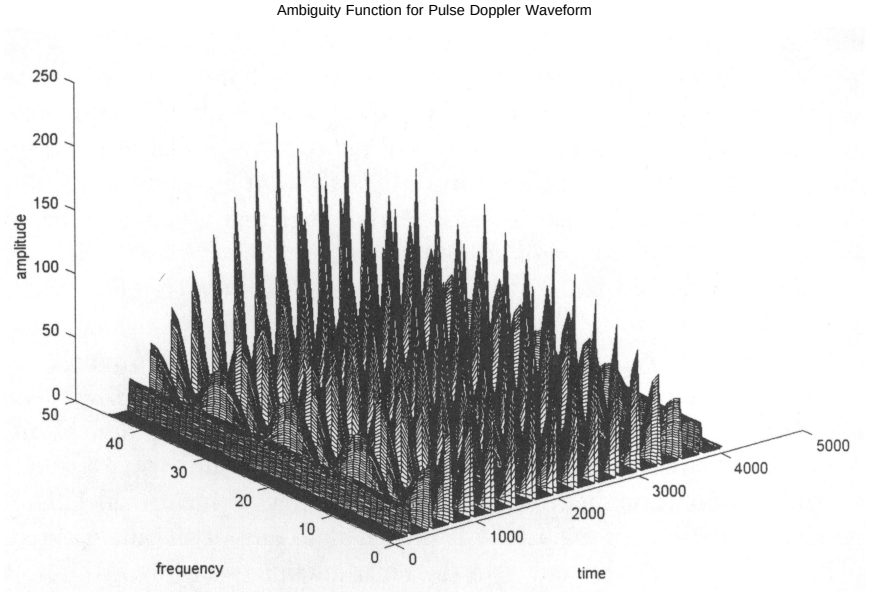

In a medium-PRF design, the number of PRFs processed during an antenna dwell time (the time the antenna takes to scan over the target) is constrained on the high side by the available processing time. If the time becomes too long, the antenna scan rate drops below an acceptable value. On the low side, the number of PRFs per dwell must be sufficient not only to resolve range but also to ensure good Doppler visibility.

An action that can reduce sidelobe clutter is to increase the radar's range resolution by narrowing the radar's effective pulsewidth and correspondingly narrowing the radar's range gates. Narrowing the radar's effective pulse width reduces the sidelobe clutter level in the same proportion by which the pulsewidth is narrowed. Additional range gates are required to provide full range coverage and more Doppler filters must be formed because a separate bank of Doppler filters is required for each range gate.

One way to narrow the effective radar pulse width without reducing the average transmitted power is PC. A common practice is to maximize the average transmitter power without incurring an unacceptable loss due to eclipsing and then use enough PC to achieve the desired range resolution. An alternative approach that minimizes eclipsing is to transmit very narrow pulses of higher peak power.

The sidelobe clutter with which a target must compete can be further reduced by narrowing the passbands of the Doppler filters. To retain all the power in the target return, the filters must be wide enough to pass the target's

spectrum. The target spectrum generally is inversely proportional to the radar's time on target (T_d) plus an allowance for internal target motion and acceleration effects.

An important form of sidelobe clutter in medium-PRF airborne radar results from large RCS targets on the ground (e.g., buildings, water towers, and other specular reflectors), which are particularly prevalent in urban or mountainous areas. Also included in this class of clutter is unwanted moving ground vehicular traffic that, because of the range and Doppler ambiguities, conflicts with the detection of airborne targets.

Although an airborne radar is vulnerable to such targets when operating at low PRF, it is more vulnerable at medium PRFs due to the severe range ambiguities in this type of operation. One way to reduce these unwanted targets is to provide the radar with a guard channel that consists of a separate receiver processor whose input is supplied by a small horn antenna mounted on the main radar antenna. The width of the horn's main lobe is sufficient to encompass the entire region illuminated by the radar antenna's principal sidelobes, and the gain of the horn's main lobe is greater than any of the main antenna's sidelobes. Any detectable target in the radar antenna's sidelobes will produce a stronger output from the guard receiver than from the main receiver. Conversely, any detectable target in the main lobe will produce a stronger signal than in the guard receiver. Consequently, by comparing the output of the two receivers and inhibiting the output of the main receiver when that of the guard receiver is stronger, we can eliminate the unwanted targets in the radar's sidelobe region.

4.2.1 EA Against PD Radar

The PD radar generally has good resistance against EA. The ability to resolve targets in Doppler frequency allows rejection of chaff and other correlated interference, which are separated from the target return by more than a Doppler filter bandwidth. The matched-filter aspect of PD operation provides the effect of coherent integration, which optimizes the target-to-jamming ratio in the presence of noise jamming. The ability of a PD radar to extract radial target velocity through direct Doppler measurement and by differentiating range measurements makes it necessary for a deception jammer to induce a realistic Doppler signature on the simulated target return. The large number of pulses generated by a PD radar provides problems for many types of EW intercept receivers that rely on deinterleaving pulse trains to identify threat radar.

The only significant disadvantage against EA is the necessity of maintaining a stable transmitter frequency and PRF for a time equal to the inverse

of the Doppler filter bandwidth. This allows a jammer the time to tune to the first transmitted pulse and then jam subsequent pulses in a spot jamming or deception mode. The vulnerability in this mode is generally to main-beam jammers, since appropriate sidelobe cancellation and blanking can be applied to reduce the effect of sidelobe jammers. Also, a sidelobe cover mode can be used whereby multiple spurious frequencies are radiated in the sidelobe direction through an auxiliary antenna at the same time that the main radar pulse is transmitted.

Efficient use of jamming ERP against a PD radar requires that the jamming waveform have sufficient correlation over the processing interval (i.e., CPI) of the PD radar to inject sufficient energy into a Doppler filter to cause it to report a target or to suppress the true target. This indicates that, from an energy viewpoint, the PD radar jammer must maintain a frequency stability greater than the Doppler filter bandwidth (i.e., 50 Hz to 500 Hz) over a time interval corresponding to the CPI time (i.e., 2 ms to 20 ms). While this might be adequate to deceive older type analog PD radars, more precise frequency control is indicated for modern PD radars using FFT digital signal processing techniques. Modern radars form multiple Doppler filters covering the frequency range of interest. Signatures of most military type targets within a particular range gate fall within a single or adjacent Doppler filter or, if due to *jet engine modulation* (JEM), have a distinctive pattern. Hence, responses in multiple Doppler filters are indications of the presence of interference or jamming signals. This forms a criterion for the purity of Doppler radar jamming signals in that they must not be detectable in multiple Doppler filters. Since Doppler filters formed digitally exhibit a sidelobe structure of the order of 20 dB to 30 dB below the main lobe, this indicates that PD jammers must not generate spurious signals above this level (i.e., 20 dB to 30 dB below the main filter response).

PD radars are used in both search and track applications. EA against PD search radars generally requires the simultaneous storage of radar signatures for many radars. This can be accomplished in several ways. The most universal is to employ a DRFM. In support jamming applications where several radars must be jammed simultaneously, this can lead to intermodulation problems and possible detection of the jamming signals (see Section 3.5). An alternate method is to employ a DDS using multiple accumulators, each tuned to a particular identified threat. This requires an extensive threat library and an accurate frequency set-on receiver (see Section 3.5). Another way is to employ multiple voltage-controlled oscillators that are locked to each threat using phased-locked loop techniques. This technique is used in several operational EA systems but is not as accurate or efficient as jammers using DDS or DRFM digital techniques.

Doppler filters in many modern radars are synthesized using the FFT. The normalized transfer function of the FFT is given [1]

$$|H(\omega)| = \left| \frac{\sin(N\omega_d T/2)}{\sin(\omega_d T/2 - k\pi/N)} \right| \tag{4.16}$$

where N is the number of pulses or FFT points, ω_d is the Doppler radian frequency, T is the interpulse interval (PRI), and k is the Doppler filter number. The FFT transfer function is illustrated in Example 4.12, where the cross-coupling between the Doppler filter channels is evident due to the high sidelobe levels of the filters (i.e., −13.3 dB for first-order sidelobe). The input to the FFT can be windowed (see Example 4.12) to produce lower sidelobes at the expense of a broader filter and less Doppler discrimination between channels. One way to implement the windowing is to post-filter-combine adjacent channels given by

$$H_\omega(\omega) = H_k(\omega) + \alpha[H_{k+1}(\omega) + H_{k-1}(\omega)] \tag{4.17}$$

where $\alpha = 0.5$ for Hanning weighting and $\alpha = 0.426$ for Hamming weighting [1]. The reduced sidelobe Doppler filters are also shown in Example 4.12 and indicate a discrimination capability of the order of 30 dB as a reasonable estimate for modern radars.

► *Example 4.12*

Using MATLAB, plot the transfer function for a bank of Doppler filters using a 32-point FFT and uniform weighting. Next, plot the transfer function for the same situation as before, but use postcombining with Hamming weighting. What is an estimate of the level of spurious content of a jamming signal that could be detected using the reduced sidelobe filters?

```
% FFT Doppler Filter Response
% ---------------------------
% fftfila.m

clf;clc;clear;

% Define Frequency Vector

N=32;      % FFT Points
PRF=2000;
```

```
T=1/PRF;
fd=(1/(2*T))*(0:1024-1)/1024;

% Compute Filter Response - Uniform Weights

for k=1:16;
x=2*pi*fd*T/2+1e-10;
H=sin(N*x)./sin(x-((k-1)*pi/N));
Hd=H.*H;
Pdb(:,k)=10*log10(Hd'/(N^2)+1e-2);
end;

% Plot Filter Response

subplot(211);
plot(fd,Pdb,'k');grid;
xlabel('Frequency - Hz');
ylabel('Amplitude - dB');
title(['FFT Filter Response - Uniform Window']);
axis([ 0 1000 -20 0]);

% Compute Filter Response - Hanning Weights

a=.5;

for k=1:16;
x=2*pi*fd*T/2+1e-10;
H(k,:)=sin(N*x)./sin(x-(k-1)*pi/N);
end;

for l=2:15;
Hw(l,:)=H(l,:)-a*(H(l+1,:)+H(l-1,:));
Hd(l,:)=Hw(l,:).*Hw(l,:);
Pldb(:,l)=10*log10(Hd(l,:)'/(N^2)+1e-6);
end;

% Plot Filter Response

subplot(212);
plot(fd,Pldb,'k');grid;
xlabel('Frequency - Hz');
ylabel('Amplitude - dB');
title(['FFT Filter Response - Hanning Weighting']);
axis([ 0 1000 -50 0 ]);
```

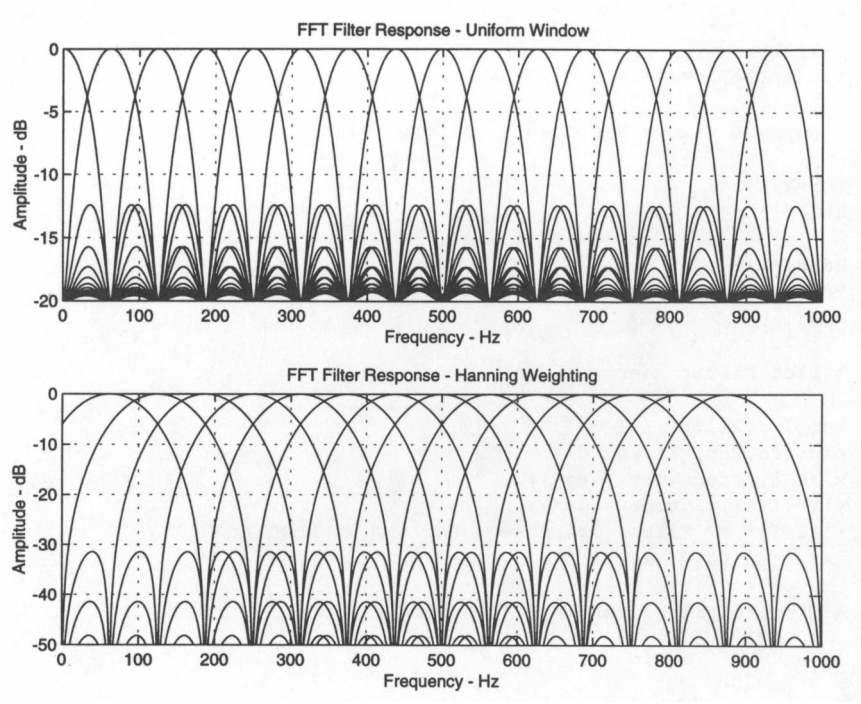

PD radars are extensively used in fire control systems to supply targeting data for missile systems. In some systems, the PD radar is located in the missile (e.g., AMRAAM) and acts to provide guidance data directly to the missile control system. Other systems using semiactive PD radars have the active PD radar that is tracking the target act as an illuminator for a bistatic receiver located in the missile. In either case, narrow "speed gates" (Doppler tracking filters) are employed to track the target. The object of the deceptive EA system is then to capture the speed gates, causing the missile to lose guidance information. This VGPO procedure is a classic technique employed against PD tracking radar and missile seekers.

VGPO is a technique used in DECM systems for use against automatic velocity tracking radars that capture the victim radar's velocity gate (speed gate), walks it off in velocity, and then turns off, leaving the radar's velocity gate with no signal. The PD radar must then go through its reacquisition mode to attempt to reacquire the target. The effectiveness of the DECM system is proportional to the time that the missile can be kept in its reacquisition mode. In modern PD radars, the use of multiple Doppler filters, formed digitally, speeds this reacquisition process and alerts the radar to the presence of jamming signals.

The bandwidth (B_d) of the speed gate must be sufficient to encompass Doppler frequency deviations caused by acceleration between the target and the missile and analog components in the servo system. This frequency deviation is given by

$$\Delta f_d = \frac{19.63 \cdot g}{\lambda B_d} \tag{4.18}$$

where g is the acceleration in g's, λ is the radar's wavelength, and B_d is the Doppler filter's bandwidth. If we balance (4.18) such that the Doppler filter bandwidth and the Doppler frequency deviation are equal for an I-band radar with a 10-g missile acceleration, then the resulting Doppler bandwidth of the "speed gate" is 80 Hz. The preceding discussion indicates that Doppler frequency bandwidths of the order of 100 Hz are reasonable for aircraft targets.

The prior discussion points to the need in DECMs that operate against PD radar to have low spurious spectral components (greater than 30 dB down from the carrier) in order to prevent detection. An examination of the DECM block diagram shown in Figure 3.5 indicates that three major components have the potential to generate spurious phase components. These are (1) the TWT microwave amplifier where incidental modulation (e.g., power supply ripple) on the helix causes phase modulation, (2) the DRFM that stretches signals through head-to-tail repetition, and (3) the serrodyne frequency offset device (see Chapter 3) that generates the deceptive Doppler signature.

Example 4.13 illustrates the effect of phase modulation on the helix of the TWT where ±4-degree peak phase modulation causes spurious components of the order of 30 dB down from the carrier at the frequency of the disturbance and its harmonics. These point to the need for good filtering of power supplies whose ripple frequencies range from 50 Hz to 400 Hz for conventional supplies to up to 100 kHz for switching power supplies.

▶ *Example 4.13*

Using MATLAB, plot a curve of the spurious spectrum levels with respect to the carrier as a function of the peak phase deviation on a helix TWT. Assume a 400-Hz ripple from the power supply modulates the carrier given by

$$v(t) = \cos\left(\omega_t + 2\pi \cdot \frac{\Delta\phi}{360} \cdot \sin(\omega_m t)\right) \tag{4.19}$$

Extend this example to multiple phase modulation components.

```
% Spurs for Helix Modulation of TWT
% ------------------------------------------
% twtspur.m

clf;clc;clear;

% Sample with fs

fs=2048;     % Hz
t=-1:1/fs:1; % sec

% Baseband and 400 Hz power supply ripple

f0=0;fm=400;         % Hz

for dfi=1:35;        % Degrees
x=exp(j*(2*pi*f0*t+dfi/360*2*pi*sin(2*pi*fm*t)));

% Find spectrum

X=fft(x,fs);
X=fftshift(X);
Pxx=X.*conj(X);

Pxx=Pxx/max(Pxx);
Pxxdb=10*log10(Pxx+1e-10);

db=max(Pxxdb(1,1:1024));

if dfi==1;xx=db;
   else xx=[xx db];end;
end;

% Plot spurs vs phase error

dfi=1:35;
plot(dfi,xx);grid;
xlabel('Peak Phase Error - Deg');
ylabel('Maximum Spur - dB');
title(['TWT Spurs for Helix Phase Modulation']);
axis([0, 35, -80, 0 ]);
```

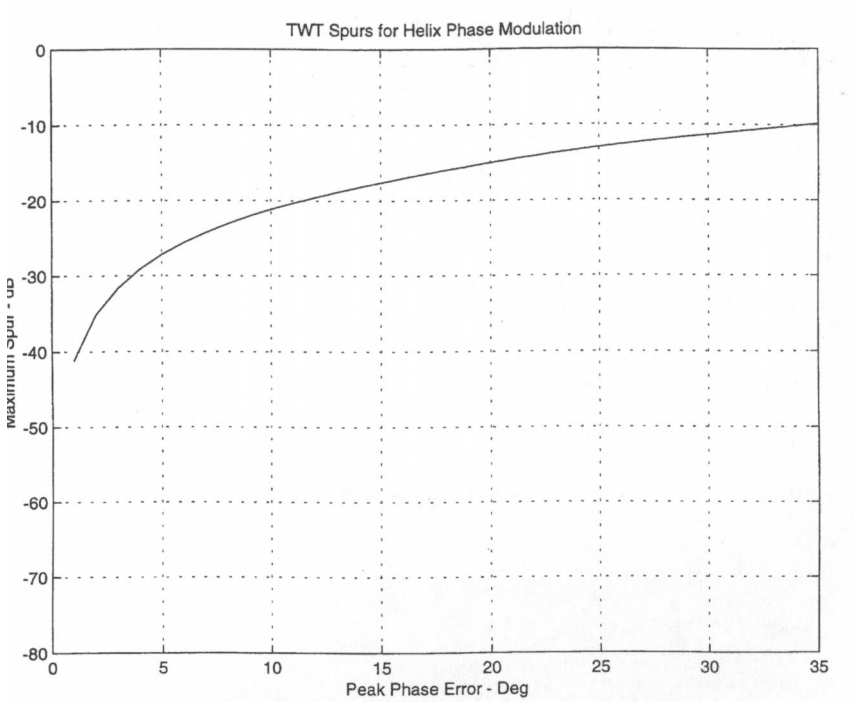

Example 4.14 indicates the spurious frequency components caused by head-to-tail stretching of stored radar signatures in a DRFM. This example illustrates that the random phase modulation using this procedure must be held to under 30 degrees to provide spurious components down 30 dB from the carrier using a 1-bit DRFM. This points to the need for development of multiple bit DRFMs and tight phase control in this type of operation.

► *Example 4.14*

Using MATLAB, find the spectrum of a CW signal that is reconstructed by storing a small segment of the signal and then repeating this portion a number of times to form the full signal. A phase discontinuity is caused by the difference between the storage time and the number of phase cycles of the signal contained within this time. Assume a 10-Hz CW signal is to be reconstructed by storing 10 segments with a 30 degree phase discontinuity. Use a storage time of each segment equal to one second.

```
% Spectrum of CW Signal Formed
% With Head-to-Tails Recirculation
% ----------------------------------
% cwspecb.m

clc;clf;clear;

% Signal parameters

w=10;          % CW signal frequency - Hz
fs=360;        % Spectrum width - Hz
dp=30;         % Phase offset - degrees

% Time vector for sample segment

t=(1:(360-fix(dp/w)))/360;

% Form head-to-tail recirculation signal

zz=[];

for i=1:10;
  x=exp(j*(2*pi*w*t));

if i==1;zz=x;
  else
zz=[zz x];end;
end;

% Find spectrum

N=10*length(t);
X=fft(zz,N);
X=fftshift(X);
Pxx=X.*conj(X);
Pxx=Pxx/max(Pxx);
Pxx=10*log10(Pxx+1e-6);
f=fs*(-N/2:N/2-1)/N;

% Plot spectrum

plot(f,Pxx);axis([-40 60 -60 0]);
title(['CW Spectrum with Recirculating '...
'  Head-To-Tails']);
xlabel('Frequency - Hz');
ylabel('Power - dB');grid;
```

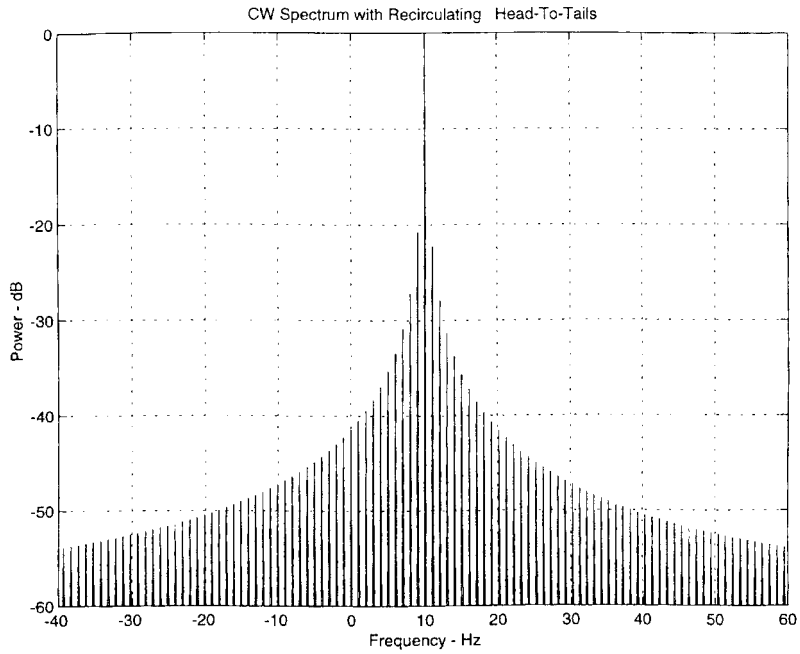

Serrodyning is a process used in DECM repeater jammers to translate the frequency of the repeated signal, thereby generating a false Doppler signal. This is accomplished by inducing a linear phase change with time, $\phi(t) = kt$ onto the signal

$$v(t) = \sin(\omega t + \phi t) = \sin(\omega + k)t \tag{4.20}$$

There are several ways that serrodyning is accomplished.

The digital phase shifter as depicted in Figure 3.8 can be stepped in phase at a linear rate, thereby causing a frequency shift in the output signal. Since the phase is stepped in discrete increments ($\Delta\phi = \pi/2^{b-1}$, where b is the number of phase bits), spurious phase components are generated in the process determined by the number of bits utilized.

▶ *Example 4.15*

Using a b-bit digital phase shifter that provides a $360/2^b$-degree phase increment per step, plot the resultant frequency spectrum for this serrodyne method. How many bits are required to ensure that the spurious spectral components are 30 dB down from the main signal?

```
% Digital Phase Shifter Serrodyning
% --------------------------------
% digserro.m

clf;clf;clear;

% Set Input Parameters

b=4;      % Quantizing Bits
N=128;    % Sample Points

% Define time vector 0 to tmax

tmax=1;
t=tmax*(0:N-1)/N;

% Sample frequency fs

fs=N/tmax;

% Define step ramp z which runs
% from 0 to tmax with amplitude 1

B=2^b;
y=B*t/tmax;
z=floor(y)/B;

% Define Phase Modulated Signal

j=sqrt(-1);
fo=0;
x=exp(j*2*pi*(fo*t+z));

% Find x for M steps

M=64;A=[];
for m=1:M;
A=[A x];end;
x=A;

% Extend for t vector

N=N*M;
t=tmax*(0:N-1)/N;

% Spectrum for x(t)

X=fft(x);
Px=X.*conj(X);
Px=fftshift(Px);
```

```
% Select central frequency axis

Px(3*N/4+1:N)=[];
Px(1:N/4)=[];
fax=fs*(-N/4:N/4-1)/N;

% Normalize amplitude

Px=Px/max(Px);
Pxdbm=10*log10(Px+1e-6);

plot(fax,Pxdbm);grid;
xlabel('Frequency - Hz');ylabel('Amplitude - dbm');
title(['Digital Phase Shifter Serrodyning' ...
'   ( Bits =',num2str(b),')']);
axis([-40 40 -60 0]);
```

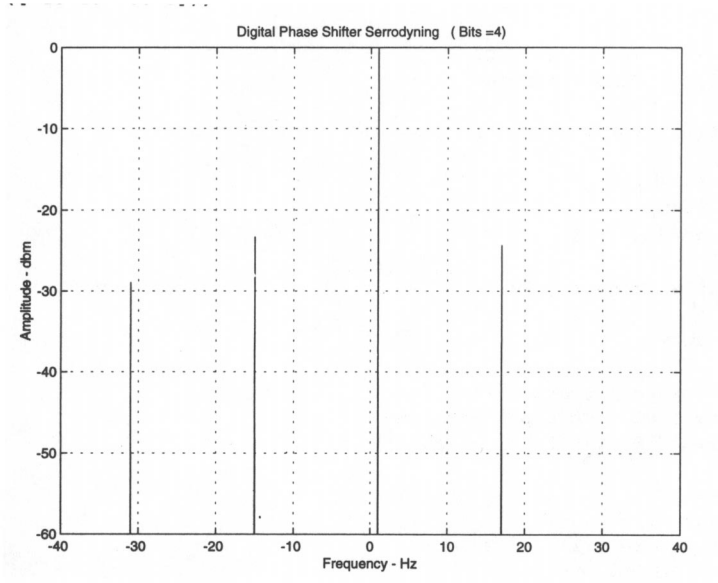

Another method for serrodyning is to modulate the helix of a TWT with a sawtooth waveform. The sawtooth amplitude must be adjusted to provide 2π-radian phase shift while its repetition rate is set at the desired Doppler frequency offset. Spurious components are caused by the finite flyback time associated with the sawtooth waveform and the deviation from 2π-radian phase shift achieved by the actual system. Example 4.16 illustrates that the flyback time of the sawtooth wave must be less than 2% of the total period for the spurious components to be 30 dB down from the output.

▶ *Example 4.16*

Plot the spectrum that results from serrodyne modulation of a TWT using a sawtooth waveform with finite flyback time so that the period is $T_1 + T_2$, where T_2 is the flyback time. What is the ratio of $T_2/(T_1 + T_2)$ that suppresses spurious components by more than 30 dB?

```
% TWT Serrodyning With Offset
% --------------------------------
% twtserro.m

clf;clc;clear;

% Set Input Parameters

r=.02;  % Ratio T2/T1+T2
N=128;  % Sample Points

% Define time vector 0 to tmax

T2=r/(1-r);
tmax=1+T2;
t=tmax*(0:N-1)/N;

% Sample frequency fs

fs=N/tmax;

% Define ramp z which runs from
% 0 to T1=1 with amplitude 1 and
% flyback from t=1 to t=1+T2

for k=1:N;
if t(k)<=1;z(k)=t(k);
else z(k)=1-(t(k)-1)/T2;end;
end;

% Plot Serrodyne Waveform

t1=tmax*(0:N)/N;
zz=z;
zz(N+1)=0;

subplot(211);
plot(t1,zz);grid;
xlabel('Time - sec');
ylabel('Amplitude');
title(['Serrodyne Waveform']);
```

```
% Define Phase Modulated Signal

j=sqrt(-1);
fo=0;
x=exp(j*2*pi*(fo*t+z));

% Find x for M steps

M=64;A=[];
for m=1:M;
A=[A x];end;
x=A;

% Extend for t vector

N=N*M;
t=tmax*(0:N-1)/N;

% Spectrum for x(t)

X=fft(x);
Px=X.*conj(X);
Px=fftshift(Px);

% Select central frequency axis

Px(3*N/4+1:N)=[];
Px(1:N/4)=[];
fax=fs*(-N/4:N/4-1)/N;

% Normalize amplitude

Px=Px/max(Px);
Pxdbm=10*log10(Px+1e-6);

subplot(212);
plot(fax,Pxdbm);grid;
xlabel('Frequency - Hz');ylabel('Amplitude - db');
title(['TWT Serrodyne Spectrum' ...
'    (Flyback Ratio =',num2str(r),')']);
axis([-30 30 -40 0]);
```

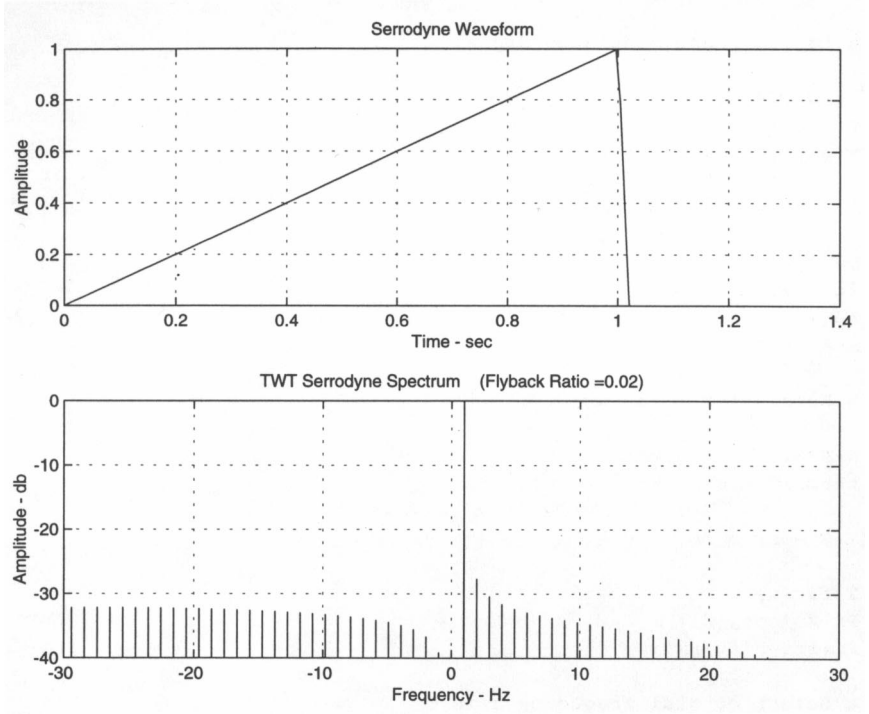

Another method of generating deceptive Doppler signals is employed in DRFMs. In DRFMs, digital storage is generally accomplished at baseband since this results in the least amount of memory for a given signal. Signals are translated to baseband by down-converting using a stable local oscillator. They are then up-converted for transmission after readout of the digital memory by up-conversion using a stable sidestep oscillator. The frequency offset between the down-converting and up-converting local oscillators corresponds to the deceptive Doppler shift induced on the signal. The generation of spurious components depends upon the stability of the oscillators and the circuitry employed in the single sideband conversion processes. These can be held to the order of 30 dB through careful design.

The tactics involved in applying deceptive Doppler signals into PD radar is dependent upon the type of PD radar involved. Low-PRF PD search radars have good range resolution capability and reject jamming signals whose Doppler is in a frequency band around the radar's PRF. Also, they usually employ PC waveforms. When the jamming technique uses false targets, both factors must be taken into account. Another technique used against low-PRF PD search radars is range-bin masking. This technique exploits the radar signal processing circuitry to suppress radar targets. As the name implies, an extended cover

pulse with a Doppler signature within the Doppler filter passband is placed over the radar target. This signal passes through the clutter rejection circuitry into the radar CFAR circuitry, which raises the detection threshold to suppress the target.

Against high- and medium-PRF PD search radars, an effective technique is to excite multiple range gates with multiple deceptive Doppler returns. This overloads the radar signal processor, which must sort out all range ambiguities to determine the true target range. One way to generate multiple Doppler targets is to divide down the radar's PRF. For example, if the radar's PRF is divided down by four (i.e., every fourth pulse repeated), then three additional deceptive targets are generated within the radar's range-Doppler matrix.

4.3 Monopulse

Generally, an effective DECM employs both range and angle deception techniques. Range deception techniques are somewhat independent of radar implementation as compared to angle deception techniques, which must be tailored to a specific radar implementation. For this reason, range deception is almost universally employed in deception jammers, but its effect is primarily limited to introducing false range information into the victim radar. While the false range information is being absorbed by the radar, it still provides accurate angle information. It is only when the radar's range gate has been captured and the DECM is turned off that angle information is denied to the victim radar. Reacquisition in the range dimension may be rapid (i.e., of the order of milliseconds) if the radar is pointed in the direction of the target. For this reason, it is appropriate to introduce false angle information into the radar at the same time RGPO is being attempted. If the radar is forced to search in both angle and range during reacquisition, then this cycle is appreciably lengthened and the radar is rendered ineffective during this period.

Modern radars and missile seekers generally use monopulse tracking systems. Monopulse tracking systems (sometimes called simultaneous lobing) form an angular-error estimate on each return pulse, thereby rendering the system insensitive to amplitude fluctuations on the data. This improves the radar performance and eliminates the possibility of amplitude modulation jamming (i.e., inverse gain) so effective against conical scanning type radar. Further, this property makes monopulse radars effective in tracking noise jamming signals that are employed against missile seekers having "home-on-jam" modes.

Monopulse tracking radars fall into three general types: amplitude-comparison or simultaneous-lobing, phase-comparison or interferometer, or a com-

bination of both types. The amplitude-comparison type involves the formation of multiple antenna beams simultaneously in space where each beam is squinted or displaced in angle from an adjacent beam. The angular measurement is made by comparing the power received in overlapping adjacent beams. An angle error is indicated by the difference in amplitude of the signals returned in the adjacent beams. The amplitude comparison can be made at any stage in the radar (RF, IF, or video), but RF comparison is typical because it provides the highest tolerance against component instability.

In phase-comparison monopulse, the antenna elements are displaced by a number of wavelengths from each other along a common baseline. If the target is located off a perpendicular bisecting the baseline, then the return signal will reach one element of the antenna before it reaches any other element. This results in a time difference between signals as they are intercepted by different elements of the antenna, which is functionally related to the angle of the target from the antenna's boresight. This time difference translates into a phase difference, which depends on the antenna element spacing and the signal's RF wavelength.

For either phase or amplitude monopulse, four antenna elements are required to provide tracking in both azimuth and elevation angles. By offsetting the antenna elements about the boresight and using a combination of phase and amplitude monopulse, it is possible to accomplish azimuth and elevation tracking using only two antenna elements. Of the three types of monopulse techniques described, amplitude monopulse is by far the most common.

Jamming techniques against monopulse radars can generally be divided into two categories. The first relies on imperfections in the monopulse design or implementation that are exploited by the jammer. These involve such techniques as image jamming, skirt frequency jamming, and cross-polarization jamming, which reverse the sense of the angle-error signal developed by the monopulse angle discriminator [1]. The second category involves multiple source techniques whose objective is to distort the EM wave's angle-of-arrival at the monopulse antenna such that either the monopulse tracker is caused to point away from the target's angular direction or spurious modulation is introduced into the tracker's servo system that causes a break-lock situation. These techniques against monopulse radars include blinking, formation jamming, cross-eye, and terrain bounce. Needless to say, it is more difficult to jam monopulse radars than sequential-lobing types (including conical scan and TWS variations). This supports the current trend in tracking radar, which is toward monopulse implementation.

In amplitude comparison monopulse the radar antenna generally forms four squinted offset antenna beams, two in azimuth and two in elevation coordinates. The monopulse pattern forms a sum pattern by combining all

beams and two difference patterns, one in azimuth and one in elevation. The radar transmitter radiates through the sum pattern while the tracking receiver uses signals that are formed through both the sum and difference antenna patterns.

Considering only the azimuth dimension (the elevation is similar), we can determine the sum and difference pattern by considering the rectangular offset apertures depicted in Figure 4.7 [6]. The sum and difference patterns are given by taking the Fourier transform of the illumination functions

$$\Sigma = (v_a(t) + v_b(t))/\sqrt{2} \tag{4.21}$$
$$\Delta = (v_a(t) - v_b(t))/\sqrt{2}$$

The resulting sum and difference antenna patterns are given in Example 4.17. Note that the sidelobes of the difference pattern are relatively high due to the use of rectangular illumination functions.

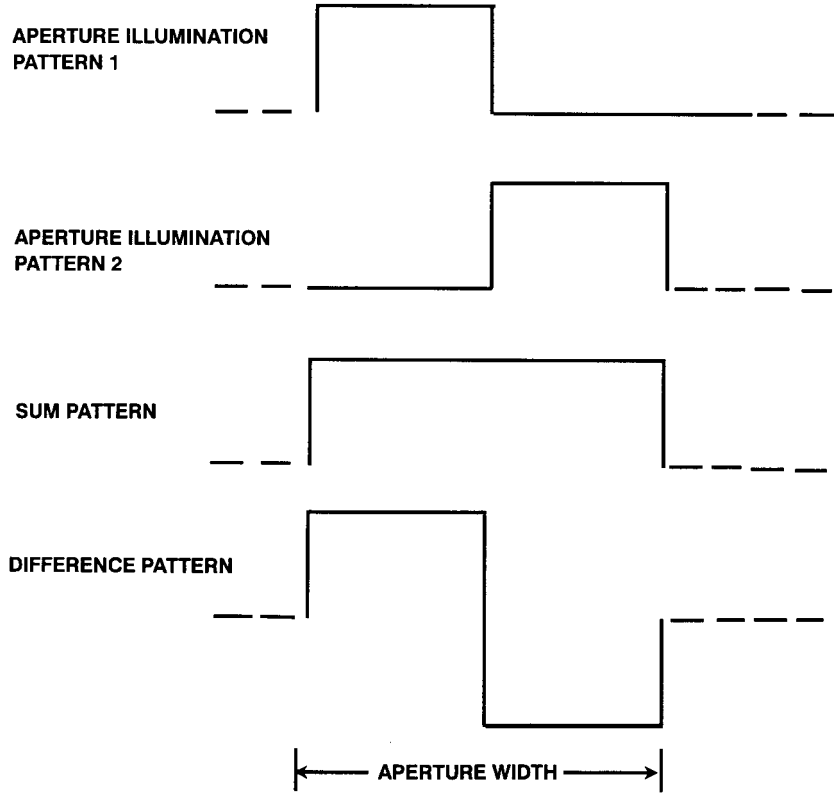

Figure 4.7 Monopulse sum and difference aperture functions.

▶ *Example 4.17*

Using MATLAB, plot the monopulse sum and difference patterns for the illumination function shown in Figure 4.7. Over what angular region of the sum pattern can the monopulse tracker lock onto the target? Is the monopulse tracking system stable when tracking in the sidelobes on a strong target or signal?

```
% Monopulse Antenna Pattern
% -------------------------
% monpat.m

clear,clc,clf;

% Normalized Aperture Width
na=4;

% Sampling Frequeny=Number elements per norm aperture
fs=8;

% Norm aperture with N elements
N=fs*na;
xna=na*(-1/2:1/(N-1):1/2);

% Illumination Function

wxna(1:N/2)=ones(1,N/2);
wxna(N/2+1:N)=-ones(1,N/2);
wxnb(1:N/2)=ones(1,N/2);
wxnb(N/2+1:N)=ones(1,N/2);

% Fill with M/2 zeros front and back

M=1024;
xna=na*(-1/2:1/N+M-1:1/2);
wxna=[zeros(1,M/2) wxna zeros(1,M/2)];
wxnb=[zeros(1,M/2) wxnb zeros(1,M/2)];

% Beam Functions from -fs/2 to fs/2 in sine space

Nfft=length(wxna);
Esine=fft(wxna,Nfft);
Esine=fftshift(Esine);

Esum=fft(wxnb);
Esum=fftshift(Esum);

% Azimuth vector

sinfi=fs/4*(-Nfft/2:Nfft/2-1)/Nfft;
```

```
% Azimuth vector in radians

fi=asin(sinfi);

% Beam gain functions

Gfi= Esine.*conj(Esine)/Nfft;
Gfs=Esum.*conj(Esum)/Nfft;

Gfi(1:Nfft/2)=sqrt(Gfi(1:Nfft/2));
Gfi(Nfft/2+1:Nfft)=-sqrt(Gfi(Nfft/2+1:Nfft));
Gfs=sqrt(Gfs);

% Plot Monopulse Antenna Pattern

plot(fi,Gfi,fi,Gfs);grid;
axis([ -.25 .25 -.8 1]);
ylabel('Amplitude');
xlabel('Angle - radians');
title(['Monopulse Antenna Patterns']);
text(.04,.8,'Sum Pattern');
text(-.22,.6,'Difference Pattern');
```

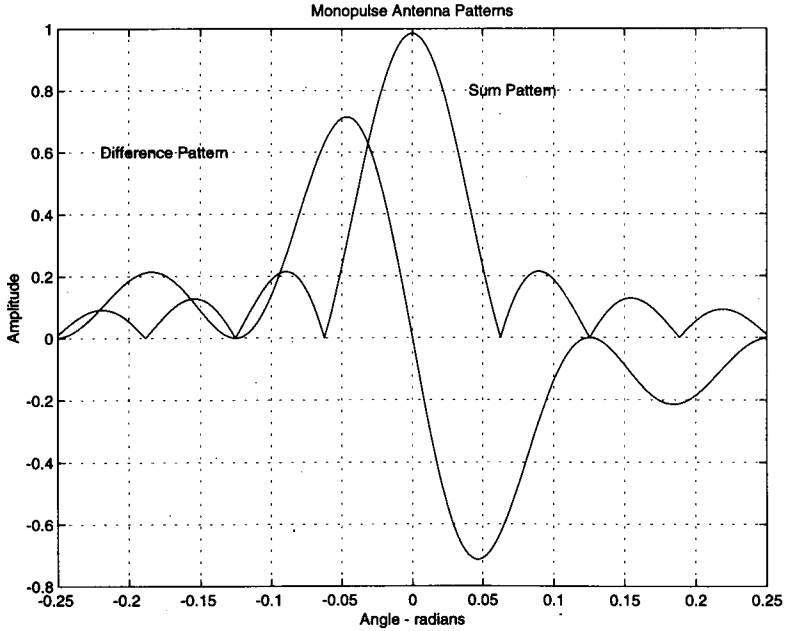

The monopulse ratio (r) is given by

$$r = \frac{|\Delta|}{|\Sigma|} e^{j\phi} \tag{4.22}$$

where Σ and Δ are the complex sum and difference voltages and ϕ is the phase angle between the sum and difference channels. Since both Σ and Δ are proportional to the target or signal strength, the monopulse ratio is independent of the amplitude of the target. In monopulse tracking systems, the real part of the monopulse ratio given by

$$\mathrm{Re}(r) = \frac{|\Delta|}{|\Sigma|}\cos\ \phi \tag{4.23}$$

is used to sense the magnitude and direction of the error between the antenna boresight and the target position. This error is then applied to a servo system that drives the antenna to null the output of the monopulse ratio detector to zero for accurate tracking. Note that when tracking a target, the monopulse antenna's boresight is driven orthogonally to the incident wave front.

From an EA viewpoint, a fundamental method for deceiving a monopulse radar in angle is through phase front distortion. Since a point source can only produce a spherical wave front, it generally is necessary to employ multiple sources to produce wave front distortion. This can be accomplished using geometrically dispersed multiple antennas or multipath signals (i.e., terrain bounce and chaff reflections) to simulate the effect of multiple antennas.

4.3.1 EA Against Monopulse Radars

The nature of monopulse tracking radars whereby angle error data are developed on each radar pulse makes them inherently difficult to jam. Some monopulse angular jamming techniques, such as skirt and image jamming and cross-polarization jamming, are designed to exploit weaknesses in the implementation of the monopulse radar. Other jamming techniques, such as cross-eye, terrain or ground bounce, and blinking or formation jamming, are designed to attack weaknesses fundamental to all monopulse tracking systems. In general, it is better to attack fundamental weaknesses rather than to rely on design weaknesses. Exploitation of design weaknesses implies a detailed knowledge of the design of the victim radar and is always susceptible to modification of the design to correct those weaknesses.

For example, image jamming, or jamming at the image frequency of the monopulse radar, depends on the fact that the phase angle at IF between two signals of the image frequency is the reverse of that which would appear at the IF if the two signals were at the normal response frequency of the receiver. In a phase-comparison monopulse system, this reverses the polarity of the error and causes the antenna to be driven away from the target if the jamming power exceeds the signal power. If the monopulse radar is equipped with an image

rejection filter or mixer, this form of jamming is rendered ineffective and hence cannot be considered as a dependable jamming technique.

Cross-polarization jamming exploits the fact that some monopulse radars give erroneous angle-error information when the received signal (jammer) is orthogonally polarized with respect to the polarization of the radar-receiving antenna. This technique exploits a design weakness generally associated with reflector-type antennas whose response to cross-polarized signals (called Condon lobes) is significantly different than that of the normal polarization response. This situation is depicted in Example 4.18, where the resulting angle-error discriminator response to the cross-polarized signal is actually the reverse of the response to the normal polarized signal. This causes the antenna to be driven away from the cross-polarized jamming signal rather than toward a signal with normal polarization.

As shown in Figure 4.8, the magnitude of the cross-polarization response is significantly reduced from that of the normal polarization response. Data on parabolic antennas indicate that the cross-polarized response is reduced by 15 dB to 30 dB with respect to the normal polarized response, while comparable data for a hyperboloid lens shows a reduction of 30 dB to 45 dB. This results in a requirement that the ratio of cross-polarized jamming power to target signal power be a minimum of 20 dB, and preferably of the order of 30 dB to 40 dB for effective cross-polarized jamming.

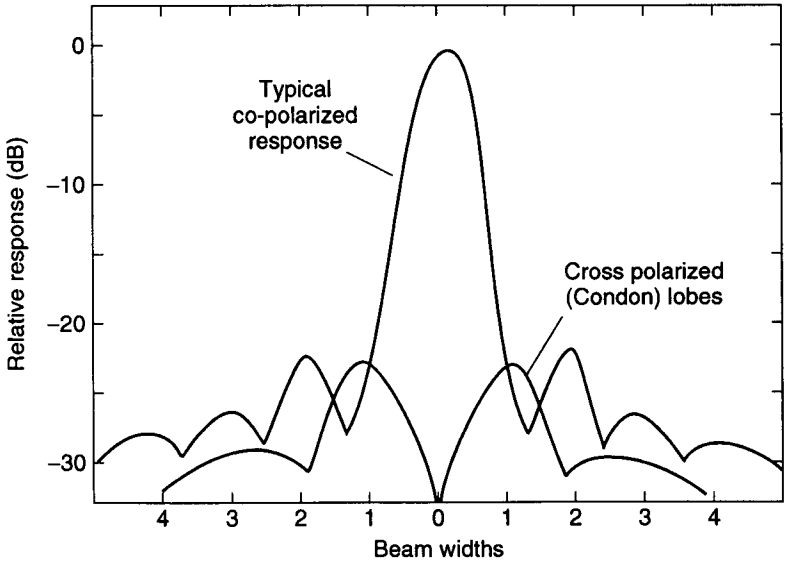

Figure 4.8 Cross-polarization response of a parabolic antenna.

In addition, any deviation in the polarization of the jamming signal from that of an exactly cross-polarized signal results in a component with normal polarization. This normal-polarized component is of the order of −41.2 dB for 0.5-degree polarization rotation, −35.2 dB for 1-degree rotation, and −29.1 dB for 2-degree deviation from orthogonality. If the normal-polarized component (which receives full response) is greater than the cross-polarized response (which is highly attenuated), then the jamming signal acts as a beacon rather than a jammer. Thus, orthogonality requirements are quite severe for cross-polarization jamming signals with requirements generally stated as ±5 degrees, which correspond to a −21.2-dB normally polarized response.

▶ *Example 4.18*

Use the fact that the cross-polarized antenna pattern is approximately 45 degrees displaced from the copolarized pattern to simulate the antenna patterns depicted in Figure 4.8 for copolarized and cross-polarized signals. Plot the difference pattern for an amplitude monopulse tracking system. Will the monopulse tracking system be stable for cross-polarized signals?

```
% Cross Polarizes Monopulse Antenna Pattern
% ----------------------------------------
% xpol.m

clear,clc,clf;

% Normalized Aperture Width

na=4;

% Sampling Frequeny=Number elements per norm aperture

fs=8;

% Norm aperture with N elements

N=fs*na;
xna=na*(-1/2:1/(N-1):1/2);

% Illumination Function

wxna(1:N/2)=ones(1,N/2);
wxna(N/2+1:N)=-ones(1,N/2);
wxnb(1:N/2)=ones(1,N/2);
wxnb(N/2+1:N)=ones(1,N/2);
```

```
% Fill with M/2 zeros front and back

M=1024;
xna=na*(-1/2:1/N+M-1:1/2);
wxna=[zeros(1,M/2) wxna zeros(1,M/2)];
wxnb=[zeros(1,M/2) wxnb zeros(1,M/2)];

% Beam Functions from -fs/2 to fs/2 in sine space

Nfft=length(wxna);
Esine=fft(wxna,Nfft);
Esine=fftshift(Esine);

Esum=fft(wxnb);
Esum=fftshift(Esum);

% Azimuth vector

sinfi=fs/4*(-Nfft/2:Nfft/2-1)/Nfft;

% Azimuth vector in radians

fi=asin(sinfi);

% Beam gain functions

Gfi= Esine.*conj(Esine)/Nfft;
Gfs=Esum.*conj(Esum)/Nfft;

Gfi(1:Nfft/2)=sqrt(Gfi(1:Nfft/2));
Gfi(Nfft/2+1:Nfft)=-sqrt(Gfi(Nfft/2+1:Nfft));
Gfs=sqrt(Gfs);

% Approximate Cross Pol Pattern

Gpc=[Gfi(1:528) -Gfi(529:1056)];

% Form Cross Pol Sum and Difference Patterns

AA=[ zeros(1,15) Gpc(1:1041)];
BB=[ Gpc(16:1056) zeros(1,15) ];

Gdif=BB-AA;
Gsum=BB+AA;

% Plot Co- and Cross Pol Paterns

subplot(2,1,1);
plot(fi,Gfs,fi,Gpc);grid;
axis([ -.25 .25 0 1 ]);
title('Co-Polarized and Cross-Polarized Patterns');
```

```
ylabel('Amplitude');
xlabel('Angle - radians');
text(.025,.9,'Co-Polarized');
text(.085,.5,'Cross-Polarized');

% Plot Co- and Cross Pol Difference Patterns

subplot(2,1,2);
plot(fi,Gfi,fi,Gdif);grid;
axis([ -.25 .25 -1 1]);
title('Co- and Cross-Polarized Monopulse Difference Patterns');
ylabel('Amplitude');
xlabel('Angle - radians');
text(.04,.6,'Cross-Polarized');
text(-.075,.8,'Co-Polarized');
```

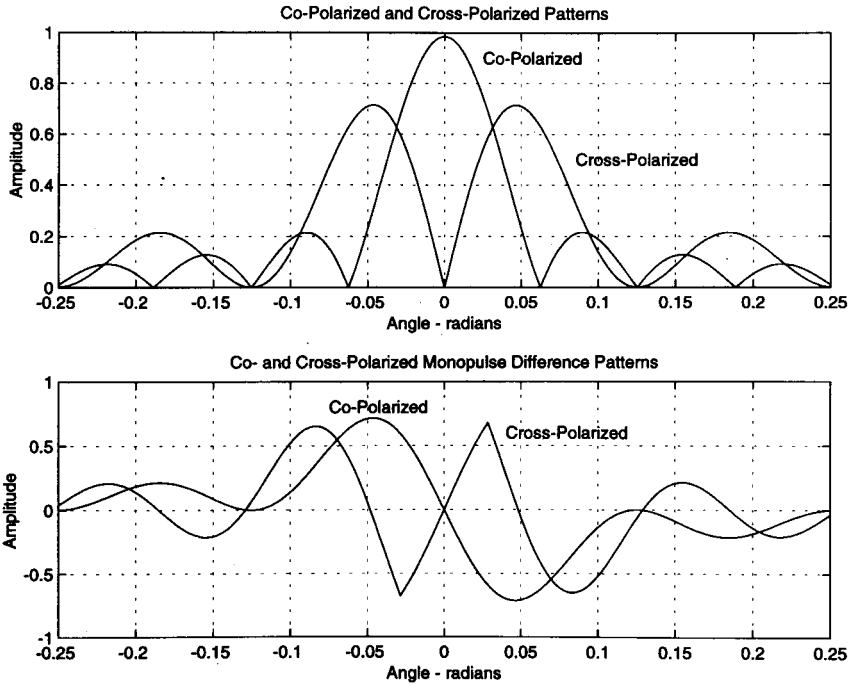

Cross-polarization jamming can be defeated by employing a radar antenna that is not susceptible to cross-polarized jamming signals. Examples of this type of antenna are flat-plate planar arrays and conventional antennas that use a polarization screen to prevent entry of the cross-polarization component. On the other hand, many radars use radomes, which tend to generate high cross-

polarization components, making them susceptible to cross-polarization jamming.

A more fundamental approach to jamming a monopulse radar, or in general, any angle-tracking radar including sequential-lobing types, is to use spatially dispersed jamming sources. The phase characteristics of the spatially dispersed jammers can be either coherently or incoherently related. Coherent jamming sources imply a deterministic or synchronized relationship between the phases of the multiple jammers, while incoherent jamming sources imply a random relationship. Coherent jammers have the unusual property that the jammer's apparent power centroid can lie in a direction that is outside the solid angle containing the jammers, while the power centroid for incoherent jammers must always lie within this solid angle.

When the jamming sources are constrained to a single platform (e.g., aircraft or ship), the solid angle subtended by the jammers is necessarily small, and coherent jamming is necessary to generate a large angular error. On the other hand, if the jamming sources are located on multiple spatially dispersed platforms, then the subtended solid angle containing the jammers is large and incoherent jamming can be used to generate large angular errors. When spatially dispersed jammers are used, only those that intercept the main beam of the tracking radar are effective.

Consider the jamming of a tracking radar by two spatially separated incoherent jammers located within the radar's main-lobe beamwidth. Under the assumption that the tracking radar's angle-error discriminator has a linear characteristic, it can be shown that the angular tracking error (θ_e) from the midpoint of the sources is given by $\theta_e = \Delta\theta \cdot (\alpha^2 - 1)/2(\alpha^2 + 1)$, where α is the relative voltage amplitude ratio of the two jammers and $\Delta\theta = L \cos \psi/R$ with L the jammer separation, R the range between the tracking radar and the midpoint of the line between the jammers, and ψ the angle between the radar pointing axis and a perpendicular to the midpoint of the line between the two jammers. This relationship indicates that if the incoherent jammer sources have equal value, the tracking radar will point at the midpoint between the sources. If one jamming source is stronger than the other, the tracking radar antenna will tend to point in a direction that is closer to the stronger source.

One form of multiple-source incoherent jamming is called formation jamming. With this type of jamming, two or more aircraft or other jamming sources (e.g., decoys or multiple reflectors) are located within the beam of the monopulse tracking radar in the same range cell. As the aspect angles to these jammers change and the various jammer signal strengths change, then the apparent direction of arrival of the composite signal will wander back and forth between the jammers. If the composite jamming signals are synchronized

to arrive simultaneously (within a range resolution cell) at the tracking radar and are sufficiently strong with respect to the skin returns from the targets carrying the jammers, then the real targets will be obscured from the tracking radar. Once separation between targets exceeds the radar beamwidth, the radar can track either target and the jammer becomes a beacon. Thus, careful coordination between the multiple jammers is required for successful formation jamming.

Another form of multiple-source incoherent jamming is called blinking jamming. This method attempts to attack the tracking dynamics of the angle-tracking radar and hence may be effective against some types of monopulse radar as well as other tracking radars. Basically, this method turns on multiple spatially dispersed jammers one at a time at a rate that is within the passband of the angle-tracking servo (e.g., 0.1 Hz to 10 Hz). As the tracking radar transfers from one jamming source to another, the step response of its angle-tracking servo is excited. If the angle-tracking servo is designed to be critically damped, then the radar antenna will smoothly move between the various jamming sources with a settling time proportional to the reciprocal of the servo bandwidth. However, if the angle tracker exhibits high overshoot (underdamped design), then exciting its servo at a rate close to its bandwidth will cause an ever-increasing perturbation, which will eventually result in the radar's breaking lock. Conversely, if the blinking rate is much higher than the angle tracker's servo bandwidth, then the angle servo will tend to average the signals from the various jamming sources, resulting in the radar antenna taking a position that corresponds to the angular center of mass of the jammers within its main-lobe antenna response.

The critical parameter with blinking jamming is the rate at which the jamming sources are commutated. Too high a rate causes the tracking radar to average the data and tends to minimize the tracking error. Too low a rate allows the tracker to accurately determine the angular position of each of the jammers. The best situation is a rate that is of the order of the tracking servo's bandwidth (e.g., 0.1 Hz to 10 Hz). However, it is not a simple problem for the jammer to attain the optimal blinking rate. One possibility is to vary the blinking rate over the range of possible values until maximum tracking error is observed at the jammer. This type of jamming is similar to that for swept audio jamming against conically scanning radar.

Coherent jamming is best performed from two synchronized sources separated by a baseline L in an interferometric configuration as depicted in Figure 4.9. From Example 4.17, it is recognized that the difference pattern Δ is approximately linear to about the 3 dB points in the sum pattern. Using this approximation, the angles measured by the monopulse tracker (θ_1, θ_2) to the two coherent jamming sources are given by

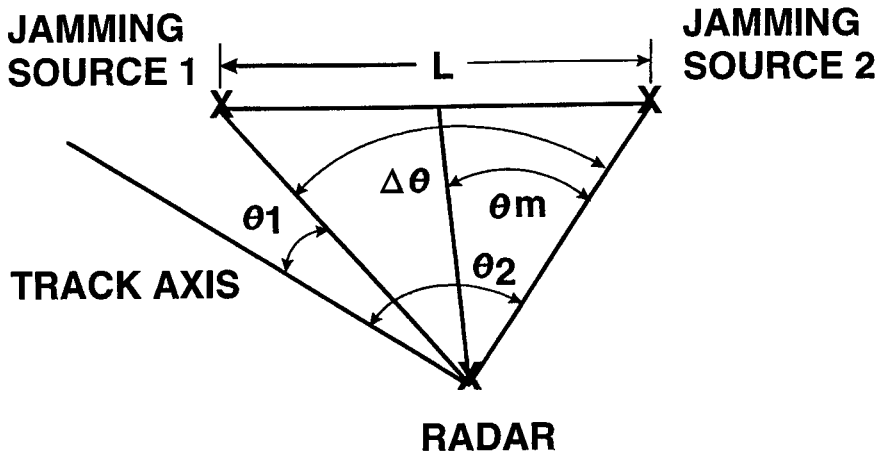

Figure 4.9 Dual-coherent source jamming.

$$\Delta_1 = km\ \theta_1\Sigma_1 \qquad (4.24)$$
$$\Delta_2 = km\ \theta_2\Sigma_2$$

where km is a scale factor. The indicated tracking angle (θ_i) of the monopulse tracker is then equal to

$$\theta_i = \frac{1}{km}\frac{\Delta}{\Sigma} = \frac{\Delta_1 + \Delta_2}{\Sigma_1 + \Sigma_2} = \frac{\theta_1\Sigma_1 + \theta_2\Sigma_2}{\Sigma_1 + \Sigma_2} \qquad (4.25)$$

The ratio Σ_2/Σ_1 can be written in complex form as

$$\frac{\Sigma_2}{\Sigma_1} = ae^{j\phi} \qquad (4.26)$$

where a is the amplitude ratio and ϕ is the phase between the jamming signals received from the two coherent jamming sources. The indicated tracking angle can then be written as

$$\theta_i = \frac{\theta_1 + ae^{j\phi}\theta_2}{1 + ae^{j\phi}} \qquad (4.27)$$

Note that at $a = 0$ (jamming source two shut-off) $\theta_i = \theta_1$ as expected. Multiplying the second term by $(1 + ae^{-j\phi})/(1 + ae^{-j\phi})$ and applying Euler's formulas results in

$$\theta_i = \theta_m - \frac{\Delta\theta}{2}\frac{1 - 2ja\sin\phi - a^2}{1 + 2a\cos\phi + a^2} \tag{4.28}$$

for the indicated angle. The real part of (4.28) indicates the indicated tracking angle of a monopulse radar subjected to dual coherent source jamming as

$$R_e(\theta_i) = \theta_m - \frac{\Delta\theta}{2}\frac{1 - a^2}{1 + 2a\cos\phi + a^2} \tag{4.29}$$

The second part of (4.29) represents the miss angle (θ_{miss}), so the miss distance is given by

$$r_{\text{miss}} = R \cdot \tan\left[\frac{\Delta\theta}{2}\frac{1 - a^2}{1 + 2a\cos\phi + a^2}\right] \tag{4.30}$$

Using the small angle approximation to $\tan(\cdot)$ and recognizing that $\Delta\theta = L\cos\psi/R$ results in a miss distance

$$r_{\text{miss}} = \frac{L\cos\psi}{2}\frac{1 - a^2}{1 + 2a\cos\phi + a^2} \tag{4.31}$$

where L is the separation between dual coherent jamming sources, a is the ratio of the amplitude of the jamming sources, ϕ is the phase difference between the jamming sources, and ψ is the angle between the radar pointing axis and a perpendicular to the midpoint of the line between the jammers.

▶ *Example 4.19*

Using MATLAB, plot (4.31) with phase (ϕ) as the abscissa and miss distance normalized to the source separation (L) as the ordinate for values of jamming amplitude ratios $a = 0.4$ to 2.5. Assume $\psi = 0$. What values of a and ϕ result in the maximum jamming effect?

```
% Normalized Miss Distance for Crosseye
% ------------------------------------
% missdis.m

clear;clc;clf;

% Input Phase Error

phi=0:.1:360; % degrees

% Input Dual Source Amplitude Ratio

for i=1:13;
a=.4+.1*(i-1);

% Compute Miss Distance

l=cos(phi*pi/180+1e-3);
r=(1-a^2)./(2*(1+2*l*a+a^2));
if a==1;r(1800)=15;end

% Plot Miss Distance

rr(:,i)=r';end;
plot(phi,rr,'k');grid;
A=max(max(rr))+1;
axis([0 360 -A A]);
title('Normalized Miss Distance for Crosseye');
ylabel('Miss Distance - r / L');
xlabel('Dual Source Phase Mismatch - degrees');
```

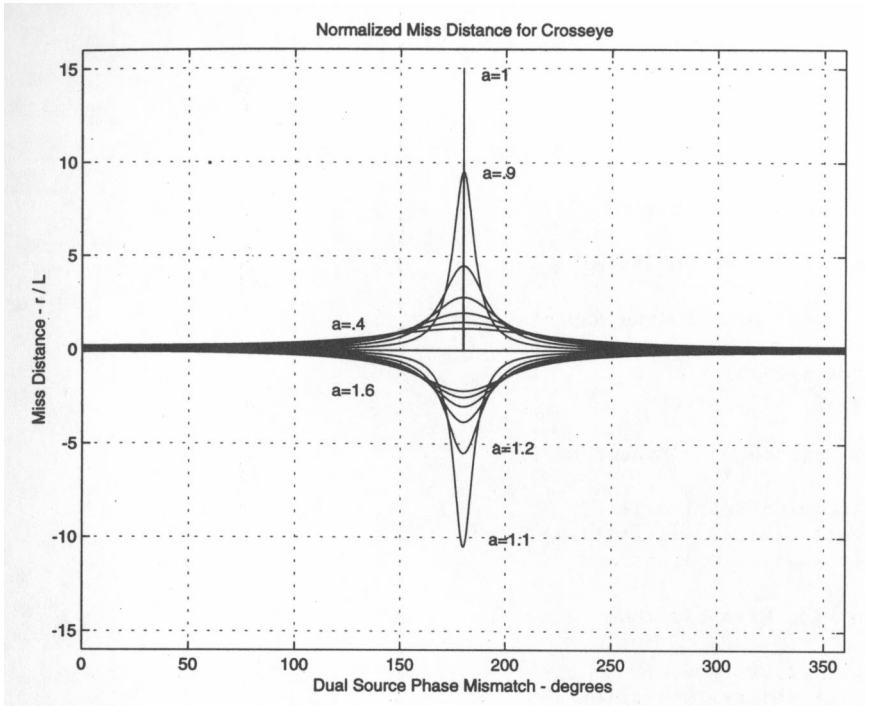

Considerable insight into the conditions for maximum jamming effectiveness can be gained by an examination of the relationship given by (4.31). First, the numerator contains a zero singularity at $a = 1$, which can only be removed by an identical singularity in the denominator. This is accomplished by setting $\phi = 180$ degrees, resulting in θ_e being proportional to $(1 + a)/(1 - a)$, which in turn is maximized for $a = 1$. Thus, the conditions that result in maximum jamming effectiveness are that the jamming sources have the same amplitude (power) and a phase separation of 180 degrees. The relationship indicates that these conditions will produce an infinite error. However, the equation applies only over the linear range of the angle-error discriminator, which generally extends only to within the radar's 3-dB beamwidth. Beyond the linear range, the angle-error discriminator saturates, which limits the angular error produced by this technique to within the radar's 3-dB beamwidth.

Now let us examine the first term in the expression for the angle error that provides insight into the sensitivity of coherent source angle jamming. The numerator is directly proportional to the interferometer source space (L) and the cosine of the angle (ψ) between a perpendicular to the interferometer baseline and the radar tracking axis. The numerator can be increased by moving the jamming sources further apart (hence, L is increased), which is the reason that jamming sources for coherent angle jamming are located on the wingtips

for aircraft installations, or on the fore and aft and port and starboard portions of naval ships. The numerator reaches its maximum value when $\psi = 0$, indicating that the jamming is most effective when the tracking radar is located broadside to the interferometric baseline. Alternatively, the jamming is ineffective when the jamming sources are in a parallel line with the tracking radar axis ($\psi = 90$ degrees). The denominator is proportional to the range (R) between the jammer and the tracking radar. This indicates that the jamming becomes increasingly effective as the range decreases, which contradicts the general expectation for most jamming situations.

Although the angular error expression gives insight into the conditions and sensitivities for maximum jamming effectiveness, it gives little insight into the particular physical phenomenon that allows large angular errors to be generated by coherent source jamming. The physical reasons are apparently related to a sharp wavefront distortion that occurs in the vicinity of interferometric nulls. Photographs of this type of distortion have been synthesized on a computer and obtained experimentally [7]. The large angular tracking error is caused as the tracking radar attempts to align itself on a perpendicular to the highly distorted wavefront.

Coherent source jamming imposes severe requirements both on the amplitude match between the sources and maintaining a phase differential of 180 degrees. To examine these sensitivities, we can separate the fundamental angle-error relationship into two terms. The first term is given by $\Delta\theta = L \cos \psi/R$, which represents the projected angle (in radians) subtended by the jamming sources as seen by the radar. The second term is a magnification factor given by $\Delta/(\Delta^2 + \delta^2)$, where $\Delta = 1 - a$ and $\delta = 180$ degrees $- \phi$ represent the deviations from the desired design values. This expression was obtained by neglecting higher order terms in both the numerator and denominator. An examination of this factor indicates that the maximum magnification is given by $1/(1 - a)$.

Consider an example of an airborne coherent source jammer whose wingtip installation is separated by 20 ft while the range is 10 nm. The jamming sources then subtend an angle of 0.33 mrad. If an angular tracking error of one degree is desired, then a magnification factor of 53 is required. This can be obtained with various combinations of a and ϕ, but assume that $a = 0.99$ is a practical value for the amplitude match. A maximum magnification of 100 is obtained when $\delta = 0$. Then it is found that a phase match of 0.54 degrees is required to obtain the desired magnification of 53. This example illustrates the high phase and amplitude stabilities required to obtain large magnification factors.

A major impediment to preserving phase coherency in dual coherent source jamming systems is the final output, high-powered TWT. The TWT *amplitude-to-phase modulation* (AM/PM) characteristic is typically 1 to 3 degrees

per dB. Therefore, as much as 45 degrees of phase shift may be obtained if the input signal varies over a 15-dB dynamic range. This inherent TWT limitation potentially can be reduced by preceding the TWT with a limiter that compresses the 15 dB to a few tenths of a decibel. Limiters in I and J bands that operate over octave bandwidths and have the necessary AM/PM characteristics are not currently available. As an alternative, limiters can be implemented at lower frequencies over minimum bandwidths of several gigahertz and translated to the higher operating frequency using mixing techniques.

The practical implementation of coherent source angle jamming uses a technique called cross-eye. A block diagram of this technique is depicted in Figure 4.10. Also shown is the geometry for an off-center-line jamming situation that motivates this particular implementation. The cross-eye technique uses two separate repeater paths. Each path contains receiving and transmitting antennas, a transmission line to connect the antennas, and an amplifier to generate the jamming signal. In addition, one path contains a 180-degree phase shifter that generates an interferometer null in the direction of arrival of the victim radar's signal. Also, phase and amplitude controls are contained in one path so that the two repeater paths can be adjusted for phase and amplitude match.

The advantage of the cross-eye implementation is that this configuration ensures that the signals radiated by the two coherent jamming sources arrive

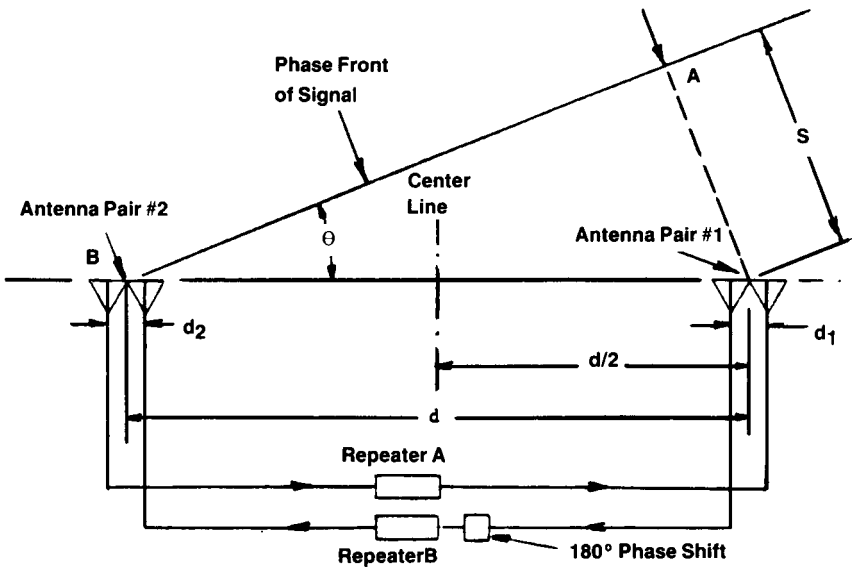

Figure 4.10 Cross-eye repeater jammer. (*Source:* [3].)

at the victim radar matched in amplitude and 180 degrees out of phase, independent of the angle of arrival of the victim radar's signal at the jammer. If the crossed configuration were not used, then a differential phase shift equal to $L \sin \psi/\lambda$ would exist between the jamming signals received at the victim radar, even though the jamming signals were matched in amplitude and 180 degrees out of phase at the jammer. This differential phase shift is caused by the additional path length (S) experienced by one jamming signal with respect to the other for off-axis signals. In the previous example, if the victim radar were at a frequency of 10 GHz, an aircraft yaw of 0.1 degree would cause a differential phase shift of about 20 degrees. If this were not compensated, the magnification factor would be reduced to a negligible amount. With the cross-eye configuration as depicted in Figure 4.10, it can be seen that both receiving and transmitting phase fronts at the jammer are parallel, thereby providing compensation for the differential phase shift caused by off-axis operation. The price paid for this compensation is an additional time delay (1 ns per foot of baseline) in the repeater path that enhances the possibility that the radar may be able to track the leading edge of the real target signal before the jammer signal arrives.

Another factor that complicates cross-eye jamming is that successful operation creates an interferometric null between the jamming signals in the direction of the victim radar. The jamming signals must compete with the real target return to capture the radar's angle tracker. To accomplish this, the angle noise caused by the real radar target must perturb the radar's antenna off the jamming signal null by an amount sufficient for a positive jamming-to-signal ratio to be generated. This results in a jamming-to-signal ratio requirement of at least 20 dB for successful cross-eye operation.

► *Example 4.20*

Given dual coherent jamming sources separated by 20m, plot the field points and phase front distortion for cross-eye jamming. Use a frequency of 9 GHz and a relative source amplitude ratio of 0.8. Plot the field pattern in a grid 8m by 0.1m centered on a perpendicular 2,000m from the line connection the dual sources. Note that the monopulse tracking antenna attempts to align itself perpendicularly to the phase front.

```
% Field Pattern for Cross-Eye Jamming
% ------------------------------------
% fieldpat.m

clear;clf;clc;

% System Parameters

a=.8;                % Dual Source Amplitude Ratio
P1=1000;G1=50;       % Jammer Source 1 ERP - w
P2=1000/a;G2=50;     % Jammer Source 2 ERP - w
L=20;                % Dual Source Separation - m
x1=-L/2;x2=L/2;
wl=3e8/9e9;          % Wavelength - 9 GHz
k=2*pi/wl;

fac1=sqrt(377*P1*G1/(4*pi)); % Field Intensity Factor
fac2=sqrt(377*P2*G2/(4*pi)); % Field Intensity Factor

% Generate Mesh Grid

N=50;
xo=0;yo=2000;          % Grid Location Center - m
dx=8;dy=.1;            % Grid Extent - m

x=-dx/2:dx/(N-1):(dx/2)*N/N-1;
y=(-dy/2:dy/(N-1):(dy/2)*N/(N-1))+yo;

[xg yg]=meshgrid(x,y);

% Generate Field Intensities

r1=sqrt((x1-xg).^2+yg.^2);
r2=sqrt((x2-xg).^2+yg.^2);

e1=fac1*sin(k*r1+pi)./r1; % Source 1 - 180 deg Phase
e2=fac2*sin(k*r2)./r2;    % Source 2 - 0 deg Phase

% Dual Source Field

e=e1+e2;

% Plot Surface Field Pattern

figure(1)
surfc(e);view([-45 45]);
title('FIELD PATTERN FOR CROSS-EYE JAMMING');
xlabel([ ' Range Field Extent ( 0.1 m )']);
ylabel([ ' Cross Range Field Extent ( 8 m )']);

% Plot Field Pattern Contour
```

```
figure(2)
contour(e,1);
title(['FIELD PATTERN CONTOUR FOR CROSS-EYE JAMMING']);
ylabel([ ' Range Field Extent ']);
xlabel([ ' Cross Range Field Extent ']);
```

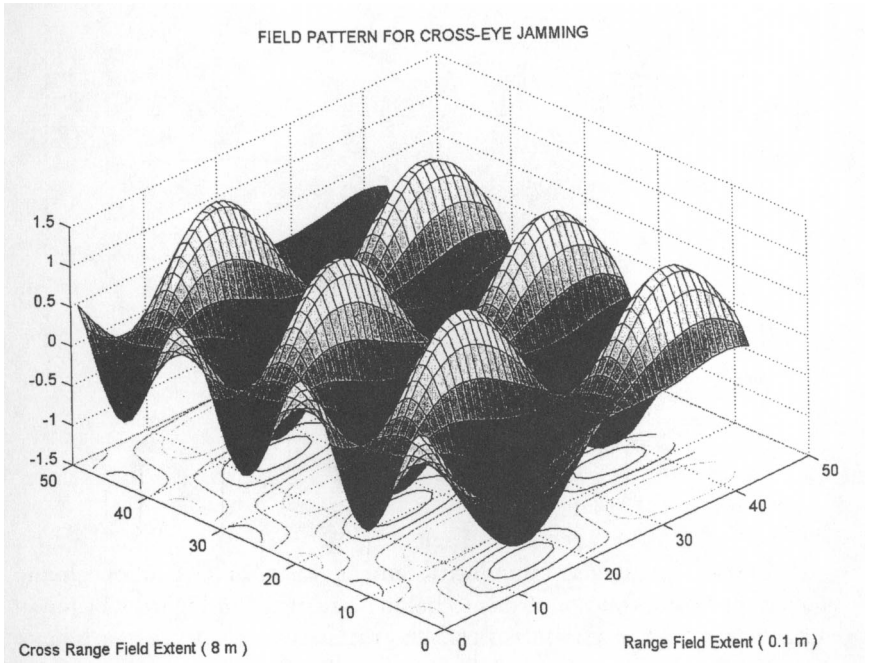

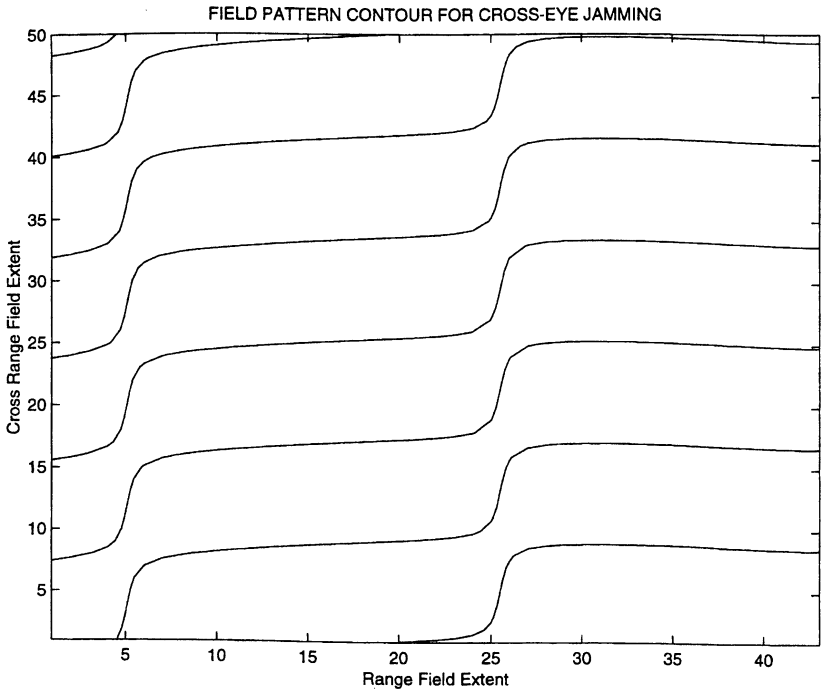

Another monopulse jamming technique is called terrain or ground bounce. The basic concept of this technique is depicted in Figure 4.11 for an engagement involving a jammer aircraft and a semiactive missile. Terrain bounce is used in the elevation plane to illuminate the Earth's surface in front of and below the jammer aircraft so that the semiactive missile angle tracker homes on the illuminated ground spot and not the jammer aircraft. The requirements

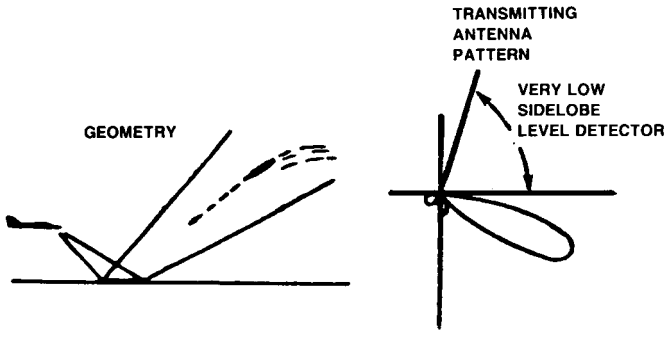

Figure 4.11 Terrain bounce jamming. (*Source:* [3].)

for terrain bounce jamming include a narrow elevation plane beamwidth, a broad azimuth beamwidth to extend the jamming coverage sector, high RF power to overcome the losses associated with the terrain propagation path, and very low sidelobes at the horizon and above to prevent the missile from beaconing on the jammer.

In addition to the terrain bounce operation depicted in Figure 4.11, it is also possible for low-flying aircraft to jam ground radar using multipath reflections from the ground. One method of accomplishing this type of operation is to form an interferometric null on the ground radar in the elevation plane in a similar manner to that used with the cross-eye technique. This prevents the ground radar from beaconing on the jammer and provides a ground bounce signal for the radar to track.

4.4 Coherent Sidelobe Cancelers

The control of sidelobe noise jamming using ultralow sidelobe antennas is not usually sufficient to completely protect a surveillance radar against sidelobe jamming. In addition, most operational radar do not use ultralow (less than −40 dB) or low (−30 dB to −40 dB) sidelobe antennas and have antenna sidelobes in the −13- to −30-dB region with average sidelobes of 0 dBi to −5 dBi. SLC is a coherent processing technique that has the potential of reducing noise jamming through the antenna sidelobes and is employed in a number of operational radars for this purpose. Present SLCs have the capability of reducing sidelobe noise jamming by 20 dB to 30 dB, but their theoretical performance is potentially much higher.

The operation of a sidelobe canceller is best understood by relating its operation to that of an adaptive antenna array processor. In an adaptive array, a weighting factor (phase and amplitude) is applied to each of the antenna elements, which are then combined in a summing network. By controlling the weighting factors through an adaptive-loop antenna pattern, nulls can be generated in any direction due to the interferometric action between any two sets of elements. Thus, the number of nulls that can be formed is equal to the number of elements minus one, which is sometimes referred to as the number of degrees of freedom of the array. The same adaptive array action can be applied to groups of elements combined into subarrays, which reduces the processing requirements for a phased array to a reasonable size. Thus, an adaptive antenna array has the potential of placing antenna pattern nulls in the direction of sidelobe jammers while still maintaining the main-lobe pattern, thereby reducing the effects of the jammer at the output port of the antenna.

While adaptive arrays are applicable to phased arrays, they are not appropriate for conventional single-element antennas. However, by adding auxiliary antennas to a conventional radar, an adaptive array type of action can be formed between the main antenna and the added antennas. This configuration is called a SLC, and the only requirement is that the auxiliary antennas must have a greater response in the direction of the jammer than the sidelobe response of the main antenna in that direction.

One of the limitations of the SLC is that the number of degrees of freedom is usually low, since only a small number of auxiliary antennas can be practically added to the main antenna (e.g., Patriot, five SLC arrays; AEGIS, six SLC arrays). Because the maximum number of sidelobe jammers that can be handled is equal to the number of auxiliary antennas, the cancellation system is easily saturated. This problem is compounded by any jammer multipath from objects in the proximity of the radar that add an additional degree of freedom for each multipath signal that has an angular direction significantly different than that of the main jammer. Another complication occurs for antennas whose cross-polarization response is significantly different than its main polarization response. This causes two orthogonally polarized auxiliary antennas to be added for each degree of freedom of the SLC system.

Sidelobe cancellation loops are best suited to cancel narrowband jamming signals. When wideband jamming signals (with respect to the radar's receiving channels) impinge on the antenna array (main and auxiliary antennas) at angles other than normal to the array, the signal appears to span an arc in angle. Thus, a single null is not adequate to cancel a wideband jammer and closely spaced multiple nulls are required in this case. Typically then, the number of sidelobe cancellation loops might be specified at up to three times the number of expected jamming sources [9]. The implementation of more than three or four cancellation loops presents a difficult operational design problem [10].

To understand the detailed operation of a CSLC, consider the block diagram depicted in Figure 4.12 [11]. Targets are received in the main antenna lobe, while jamming interference is received in the antenna's sidelobe response. Jamming signals are also intercepted in a number of auxiliary antennas whose gain in the direction of the jammers exceeds that of the sidelobe gain of the main antenna. It is further assumed that the target signals intercepted in the auxiliary antennas are insignificant compared to the jammer's strength. This is generally a good assumption, but in some implementations a directive auxiliary antenna is employed to enhance the jamming signals.

The jamming signals intercepted in each auxiliary antenna are weighted in amplitude and phase (i.e., complex weights) to form a sum that is then subtracted from the signal in the main antenna. The weights are controlled by an adaptive processor to minimize the jammer signal power at the output

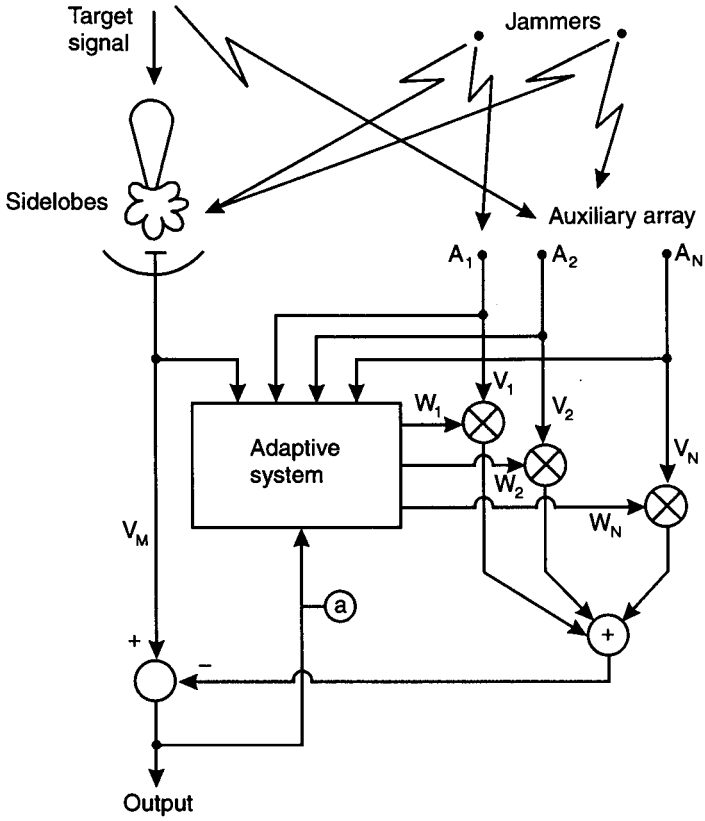

Figure 4.12 Coherent sidelobe canceller block diagram. (Farina, A., *Electronic Counter-Countermeasures,* © 1990 McGraw-Hill.)

of the system. In effect, if the CSLC performs optimally, it will adjust its weights so that the jammer signals in the main antenna are completely canceled by the jamming signals received in the auxiliary antenna.

In the absence of receiver noise, the signal at the output of the CSLC is composed of three components

$$\mathbf{Z} = \mathbf{S} + \mathbf{J} - \mathbf{J}_a^{\mathrm{T}}\,\mathbf{W} \tag{4.32}$$

where $\mathbf{S}$ is the signal vector, $\mathbf{J}$ is the jamming signal vector, $\mathbf{J}_a^{\mathrm{T}} = (J_{a1}, J_{a2}, \ldots, J_{ak})$ is the jamming signal in the auxiliary antennas, and $\mathbf{W} = (w_1, w_2, \ldots, w_k)$ are the complex weights. The CSLC power output is given by

$$P_z = E(Z^2) = P_S + P_j - 2\mathbf{P}^{\mathrm{T}}\mathbf{W} + \mathbf{W}^{\mathrm{T}}\mathbf{R}\,\mathbf{W} \tag{4.33}$$

where P_S is the signal power, P_j is the jamming power in the main lobe, $\mathbf{P}^T = E(\mathbf{J}\,\mathbf{J}_a^T)$, and $\mathbf{R} = E(\mathbf{J}_a\,\mathbf{J}_a^T)$ is the jammer's covariance matrix.

Using the orthogonality principle, the optimal weights result when the data is orthogonal with the error

$$E(\mathbf{Z} \cdot \mathbf{J}_a) = E((\mathbf{S} + \mathbf{J} - \mathbf{J}_a^T\,\mathbf{W}) \cdot \mathbf{J}_a) = 0 \tag{4.34}$$

Performing the indicated operations and noting that the signal and jammer signals are uncorrelated results in

$$\mathbf{P} - \mathbf{R}\,\mathbf{W} = 0 \tag{4.35}$$

The optimal weights for best cancellation are then

$$\mathbf{W}_0 = \mathbf{R}^{-1}\mathbf{P} \tag{4.36}$$

Substituting (4.36) into (4.33) results in

$$P_Z = P_S + P_j - \mathbf{P}^T\mathbf{W} \tag{4.37}$$

The jammer residual power at the CSLC is given by $\Delta J = P_j - \mathbf{J}_A^T\,\mathbf{W}$, so the *cancellation ratio* (CR) equals

$$CR = \frac{P_j}{P_j - \mathbf{P}^T\mathbf{W}} \tag{4.38}$$

If $P_j = \mathbf{P}^T\mathbf{W}$, the cancellation is perfect.

When noise is present, the CSLC output signal becomes

$$\mathbf{Z} = \mathbf{S} + (\mathbf{J} + \mathbf{N}) - (\mathbf{J}_a + \mathbf{N}_a)^T\mathbf{W} \tag{4.39}$$

where $\mathbf{N}$ is the main and $\mathbf{N}_a$ the auxiliary channel noise vectors. Applying the orthogonality theorem to determine the optimal weights results in

$$\mathbf{W}_0 = (\mathbf{R} + \sigma_n^2\,\mathbf{I})^{-1}\mathbf{P} \tag{4.40}$$

and the cancellation ratio becomes

$$CR_n = \frac{P_j}{P_j - \mathbf{P}^T(\mathbf{R} + \sigma_n^2\mathbf{I})^{-1}\mathbf{P}} \tag{4.41}$$

where σ_n^2 is the receiver noise power in the main channel and **I** is the identity matrix.

For a single auxiliary antenna CSLC, the covariance matrix for no noise degenerates to the scalar

$$R = E(J_1^2) = \sigma_j^2 \tag{4.42}$$

where σ_j^2 is the jammer's power. We assume a Gaussian correlation function given by

$$\rho = \exp(-(\Delta t/\tau_c)^2) \tag{4.43}$$

where Δt is the differential time between the jamming signal in the main and auxiliary channel and $\tau_c = 1/B_c$ where B_c is the channel's bandwidth. The differential time of arrival Δt is given by

$$\Delta t = \frac{d \sin \theta}{c} \tag{4.44}$$

where d is the distance between the main and auxiliary antennas and θ is the angle the jammer makes with respect to a perpendicular from a line connecting the two antennas. The cross-correlation $\mathbf{P}^T$ between the main and auxiliary jamming signals is then found as

$$P = E[\mathbf{J}\ \mathbf{J}_1] = \rho\ \sigma_j^2 \tag{4.45}$$

The optimal weight is given by

$$\mathbf{W}_0 = \mathbf{R}^{-1}\mathbf{P} = \rho/\sigma_j^2 \tag{4.46}$$

resulting in a cancellation ratio for a single CSLC with no noise of

$$CR_1 = \frac{\sigma_j^2}{\sigma_j^2 - \sigma_j^2\rho^2} = \frac{1}{1-\rho^2} \tag{4.47}$$

Table 4.1 tabulates the single CSLC cancellation ratio without receiver noise for various values of the correlation coefficient ρ.

When receiver noise (σ_n^2) is present in the single CSLC, then $R = \sigma_j^2 + \sigma_n^2$ and $P = \rho\sigma_j^2$, resulting in an optimal weight of

Table 4.1
Single CSLC Cancellation Ratios for Various Correlation Coefficient Values (No Noise)

ρ	CR_1 (dB)
0.9	7.2
0.99	17
0.999	27
0.9999	37

$$W_0 = \frac{\rho\sigma_j^2}{\sigma_j^2 + \sigma_n^2} = \alpha\rho \tag{4.48}$$

where

$$\alpha = \frac{\sigma_j^2}{\sigma_j^2 + \sigma_n^2} = \frac{JNR}{1 + JNR} \tag{4.49}$$

The cancellation ratio then becomes

$$CR_1 = \frac{\sigma_j^2}{\sigma_j^2 - \sigma_j^2\alpha\rho^2} = \frac{1}{1 - \alpha\rho^2} \tag{4.50}$$

Table 4.2 tabulates the single CSLC cancellation ratios with receiver noise for various values of the correlation coefficient ρ.

An examination of Table 4.2 indicates that jamming signals can only be canceled using CSLCs to the noise level when a perfect correlation between

Table 4.2
Single CSLC Cancellation Ratios for Various Correlation Coefficient Values
(JNR = σ_j^2/σ_n^2)

	CR (dB) for JNR =				
ρ	10 dB	20 dB	30 dB	40 dB	∞
0.9	5.8	7.0	7.2	7.2	7.2
0.99	9.6	15.3	16.8	17	17
0.999	10.3	19.3	25.2	26.8	27
1	10.4	20	30	40	∞

the jamming signals in the main and auxiliary channels exists. With imperfect correlation and high JNRs, the jamming signals will exceed the receiver noise level by a considerable amount.

Analysis of the performance for a double CSLC with receiver noise can be performed using the general formulations given in (4.39) to (4.41). The covariance matrix becomes

$$\mathbf{R} = (\sigma_j^2 + \sigma_n^2)^2 \begin{bmatrix} 1 & \alpha\rho^4 \\ \alpha\rho^4 & 1 \end{bmatrix} \tag{4.51}$$

while the cross-correlation becomes

$$\mathbf{P}^T = \sigma_j^2 [\rho \ \rho] \tag{4.52}$$

The resulting optimal weights are

$$\mathbf{W}_0^T = \begin{bmatrix} \dfrac{\alpha\rho}{1 + \alpha\rho^4} & \dfrac{\alpha\rho}{1 + \alpha\rho^4} \end{bmatrix} \tag{4.53}$$

The cancellation ratio can be found as

$$CR_2 = \frac{1 + \alpha\rho^4}{1 + \alpha\rho^4 - 2\alpha\rho^2} \tag{4.54}$$

Table 4.3 tabulates the double CSLC cancellation ratios with receiver noise for various values of the correlation coefficient ρ. It indicates that increased cancellation ratios are available with a double CSLC as compared to a single CSLC.

Table 4.3
Double CSLC Cancellation Ratios for Various Correlation Coefficient Values
(JNR = σ_j^2 / σ_n^2)

	CR_2 (dB) for JNR =				
ρ	10 dB	20 dB	30 dB	40 dB	∞
0.9	11.1	15.6	16.5	16.6	16.6
0.99	13.1	22.7	31.5	36	36.9
0.999	13.2	23.0	33	42.8	51
1	13.2	23.0	33	43	∞

Note that the preceding analysis assumes that optimum weights are achieved by the CSLC. When closed-loop CSLCs are employed, high loop gain is required to allow optimal weights to be achieved. Also, the settling time to achieve optimal weight settings are a function of the strength of the jamming waveforms.

► *Example 4.21*

Using MATLAB, plot the cancellation ratios achieved with single and double CSLC for various correlation coefficients (ρ = 0.9 to 0.9999) with no noise and a *JNR* = 10 dB to 50 dB.

```
% Cancellation Ratio for CSLC
% --------------------------
% cslcpera.m

clear;clc:clf;

% Input Correlation Coefficients

e=1:5;
rhox=1-1./10.^e;

% Input Jam-to-Noise Ratio in DB

jnrdb=10:50;
jnr=10.^(jnrdb/10);

% Calculate Single Loop CR

for i=1:5;
rho=rhox(i);
a=jnr./(jnr+1);
cr1=1./(1-a*rho^2);
cr1db=10*log10(cr1);
CR1(:,i)=cr1db';
end;

% Plot Single Loop CR

subplot(1,2,1),
plot(jnrdb,CR1);grid;
title('CSLC Cancellation Ratio - Single Loop');
xlabel('Jam-to-Noise Ratio - dB');
ylabel('Cancellation Ratio - dB');

% Calculate Double Loop CR

for i=1:5;
rho=rhox(i);
```

```
a=jnr./(jnr+1);
cr2=(1+a*rho^4)./(1+a*rho^4-2*a*rho^2);
cr2db=10*log10(cr2); CR2(:,i)=cr2db';
end;

% Plot Double Loop CR

subplot(1,2,2),
plot(jnrdb,CR2);grid;
title('CSLC Cancellation Ratio - Double Loop');
xlabel('Jam-to-Noise Ratio - dB');
ylabel('Cancellation Ratio - dB');
```

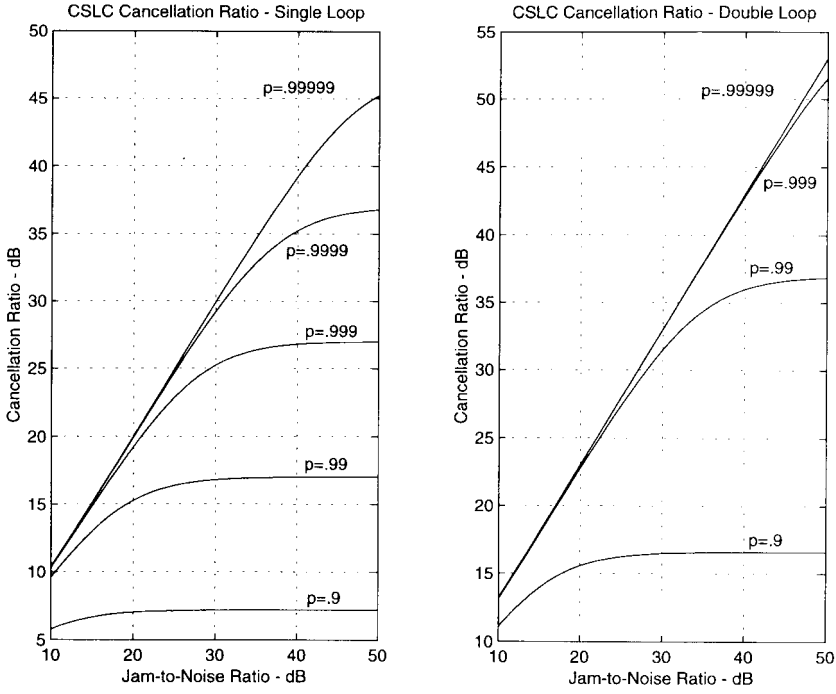

4.4.1 EA Against Coherent Sidelobe Cancelers

The CSLC has a number of inherent defects that can be exploited by support jammers. First, as previously discussed, the number of degrees of freedom in a CSLC is generally limited. Thus, if multiple jamming signals can be induced into the jammer at various angles through, for example, multipath reflections, then the CSLC becomes overloaded and its performance becomes severely degraded.

Another factor that affects CSLC performance is any decorrelation that exists between the jamming signals observed in the main antenna channel and those in the auxiliary antenna channels. This decorrelation becomes prevalent when the bandwidths of the two channels are mismatched as generally occurs since the main channel is matched to receive the radar targets while the auxiliary channel is matched to receive the jamming waveform. An examination of Tables 4.1 through 4.3 shows that performance degrades rapidly when decorrelation occurs.

Perhaps the most vulnerable characteristic of CSLCs is their transient response. Most CSLCs are designed to counter CW jamming signals. As such, they employ servo loops with narrow bandwidths that take a long time to settle. Generally, CSLCs are supplemented with sidelobe blankers that function to blank pulse signals. However, the sidelobe blanker must be judiciously employed because if it functions against a CW signal, it would enhance the jamming by blanking all the targets. A jamming technique that is often effective against radar is the transmission of multiple synchronized false targets in the sidelobe region. The CSLC cannot respond to these targets because of its transient response; but if a sidelobe blanker is employed, it will blank any main-lobe target that corresponds to a false sidelobe target.

Another support jamming tactic that attempts to exploit the transient behavior of the CSLC is to employ blinking jamming. Blinking refers to the synchronized commutation of jamming transmissions among a group of spatially displaced jammers. When properly timed, the various closed loops associated with each auxiliary antenna in a CSLC will never settle to a steady-state condition, thus severely degrading its performance.

A more general vulnerability of the CSLC is the cross-polarization response of the main and auxiliary antennas. If these are not matched, as is generally the case, then the CSLC will not cancel the copolarized interference. This is of particular concern if the main antenna has a large copolarized response since most jammers employ either circular or slant polarized jamming radiations with large cross-polarized components. To protect against this situation, many radars employing CSLCs have both vertical and horizontal auxiliary antennas to allow for cancellation of both the vertical and horizontal components of the jamming signal.

Another EA tactic that has been suggested using cross-polarization jamming attacks the sidelobe blanking system that is generally associated with CSLC systems [12]. This main-lobe jamming technique generates alternating polarization jamming cover pulses that are switched within a radar pulse width. The cross-polarized response of the main antenna is generally nulled for a jamming signal in the direction of the antenna's boresight. The higher cross-polarization response in the auxiliary antenna will activate the sidelobe blanker, which will partially blank the real target return, thereby limiting detection.

4.5 Problems

1. A PC radar transmits a 40-μs linear FM pulse with 25-MHz bandwidth. The radar has a 5-dB noise figure and produces a 20-dB signal-to-noise ratio at the radar receiver output on a 10-m^2 target. What jammer power at the radar receiver output is required to produce a 0 dB jam-to-signal ratio? How does this compare to the jamming power that would be required if the linear FM chirp waveform is replaced with a conventional pulse of the same duration?

2. Assume that both the PC and conventional radar in Problem 1 employ pulse-to-pulse frequency agility with 200-MHz bandwidth. How do the relative jamming powers required for 0 dB jam-to-signal ratio now compare?

3. Consider a binary phase code modulated radar with 50-kW power output at 5.5 GHz, 36-dB antenna gain, 10-MHz chip bandwidth, and a PC ratio of 128. Further assume that a 200-MHz main beam broadband noise jammer provides 10-dB jam-to-signal ratio before the matched filter. What is the burn-through-range of the radar?

4. For the radar in Problem 3, assume that main beam support jamming with 200-W power and 10-dB antenna gain is located 60 km from the radar. What is the burnthrough range if CW jamming tuned to the carrier frequency of the radar is employed?

5. Using MATLAB, plot the ambiguity function for a 13-bit Barker-coded PC waveform.

6. A 10-GHz pulse Doppler radar transmits 3 kW of average power at a PRF of 300,000 pulses per second. Its antenna gain is 35 dB and it processes targets using a 2048-point FFT that employs Hamming weighting (processing loss is 3.1 dB, 3-dB bandwidth is 1.3 with respect to uniform weighting). The noise figure is 4 dB. Find the maximum range at which a 2-m^2 target produces a 15-dB signal-to-noise ratio assuming the only loss is the windowing loss.

7. A noise jammer with 10-MHz bandwidth is located on the target detected by the radar in Problem 6. What jammer ERP is required to reduce the detection range to 2 km (signal-to-jam ratio of 15 dB)? Assume that radar and jammer losses are equal except for the windowing loss and that the jammer has a 3-dB polarization loss.

8. A DRFM is used on the jammer of Problem 7 to concentrate jamming energy into the Doppler filter containing the target. What ERP is now required to reduce the detection range to 2 km? How does this compare with the ERP required by the noise jammer?

9. A 10-GHz aircraft radar illuminates a target for a semiactive radar homing missile. The radar illuminator transmits 4-kW CW and has 33-dB gain. The missile seeker uses a 50% efficient 6-in-diameter circular array, has 500-Hz effective bandwidth, and 9-dB receiver noise figure. If a 4-m^2 target

is 20 nmi from the illuminator, find the range at which the missile can effectively track the target assuming a 20-dB signal-to-noise ratio is required. Assuming a noise jammer with 1-MHz bandwidth is used to protect the target aircraft, what jammer ERP is required to reduce the target lock-on range to 1 nmi assuming the only loss is a 3-dB jammer polarization loss?

10. To prevent the seeker in Problem 9 from tracking the noise jammer, assume that a swept velocity noise waveform is used to capture the seeker's speed gate. This sweeps bandpass noise through the expected Doppler band covered by the seeker. What is the maximum Doppler frequency seen by the seeker assuming that the target and illuminating aircraft travel at 500 knots and the missile at 1000 knots? What frequency range should be swept by the jammer? What bandpass and sweep rate should be used? How much jammer ERP is required if a jam-to-signal ratio of 20 dB is necessary to capture the seeker's speed gate?

11. Develop a MATLAB program for a step approximation of a linear FM chirp waveform that might be used in a DRFM to conserve memory space. Sample the chirp given in Example 4.1 at eight equally spaced intervals. Then reconstruct the chirp by filling in the missing portions of the waveform in a head-to-tails manner as in Example 4.14. Use a random phase discontinuity in the reconstructed waveform of 30 degrees for each segment. Then replot and compare the spectrum and matched filter output as shown in Example 4.1.

12. Using the MATLAB program for digital phase shifter serrodyning given in Example 4.15, plot the peak spurious level versus the number of phase shifter bits from 1 to 8.

13. Generate an amplitude monopulse difference pattern by subtracting two sin x/x patterns separated by their 3-dB beamwidth. Show that the sign of the error signal is always correct in the sidelobes. Will this be true for other beam spacings? For what other antenna patterns will this not be true?

14. Assume it is desired to defend a naval ship against an ASCM using a monopulse seeker. A cross-eye system is to be used. The cross-eye antennas have a baseline of 30m, while the ship length is 600m. The phase mismatch is 1/2 degree. What amplitude mismatch ratio is required to cause the monopulse seeker to point off the ship at a range of 1 km?

15. The Condon lobes of a monopulse parabolic reflector antenna have a magnitude 20 dB down from the peak of the main lobe. A cross polarization jammer is used against the monopulse tracking system. What is the maximum polarization mismatch that can be tolerated to prevent the jammer from acting like a beacon instead of a jammer?

16. Cassegrain twist reflector antennas are used on several antiship missile seekers to protect against cross-polarization jamming. A fixed vertically polarized

monopulse feed structure illuminates a fixed parabolic reflector formed using a vertical wire grid. The reflected wave is then directed against a flat plate twist reflector that changes the antenna's polarization from vertical to horizontal. The horizontally polarized wave is then radiated through the transparent parabolic reflector. Discuss how this configuration is resistant to cross-polarization jamming.

17. The reduction of radar detection range due to noise jamming can be deduced as $[(J + N)/N]^{1/4}$, where J is the jamming power and N is the noise power at the receiver terminals. Plot the range reduction factor as a function of the ratio of jammer-plus-noise to noise.

18. Assume that a radar requires a 20-dB signal-to-noise ratio for reliable target detection at maximum radar range. A noise jammer operates in a radar sidelobe that is 20 dB down from the main lobe response. What jam-to-signal power is required to reduce the radar detection range to 30% of its full value (see Problem 17)? What sidelobe cancellation ratio is required to restore the detection range to 70% of its full value?

References

[1] Schleher, D. C., *MTI and Pulsed Doppler Radar,* Norwood, MA: Artech House, 1986.

[2] Neri, F., "New Technologies in Self-Protect Jammer," *J. Electronic Defense,* July 1991.

[3] Schleher, D. C., *Introduction to Electronic Warfare,* Norwood, MA: Artech House, 1986.

[4] Harris, F., "On the Use of Windows for Harmonic Analysis with the Discrete Fourier Transform," *IEEE Proc.,* Vol. 66, No. 1, Jan. 1978.

[5] Berkowitz, R., *Modern Radar,* New York: John Wiley, 1965.

[6] Sherman, S., *Monopulse Principles and Techniques,* Norwood, MA: Artech House, 1984.

[7] Dunn, J., and D. Howard, "Target Noise," in M. I. Skolnik (ed.), *Radar Handbook,* New York: McGraw-Hill, 1970.

[8] Hyberg, P., "Radar Countermeasure Technology," A Compendium for the Swedish Military Academy, FOA Report A 10052-1.1, Dec. 1993.

[9] Chapman, D., "Adaptive Arrays and Sidelobe Cancelers: A Perspective," *Microwave J.,* Aug. 1977.

[10] Prior, J., and N. Woodward, "Performance of Current Radar Systems in an EW Environment," *Military Micro Conf.,* 1976.

[11] Farina, A., and F. Studer, "Evaluation of Sidelobe Canceller Performance," *IEEE Proc.,* Vol. 129, Pt. F, No. 1, Feb. 1982.

[12] Van Brunt, L., *Applied ECM,* Volume 2, Dunn Loring, VA: EW Engineering, 1982.

[13] Povejsil, D., R. Raven, and P. Waterman, *Airborne Radar,* Princeton, NJ: Van Nostrand, 1961.

[14] Skolnik, M., *Radar Handbook,* 2nd Ed., Ch. 9, New York: McGraw Hill, 1990.

[15] Weher, D. R., *High Resolution Radar,* Norwood, MA: Artech House, 1987, p. 139.

[16] Long, M. W., "Medium PRF for the AN/APG-66 Radar," *Proc. of the IEEE.*

[17] Stimson, G. W., *Introduction to Airborne Radar,* El Segundo, CA: Hughes Aircraft Company, 1983, p. 448.